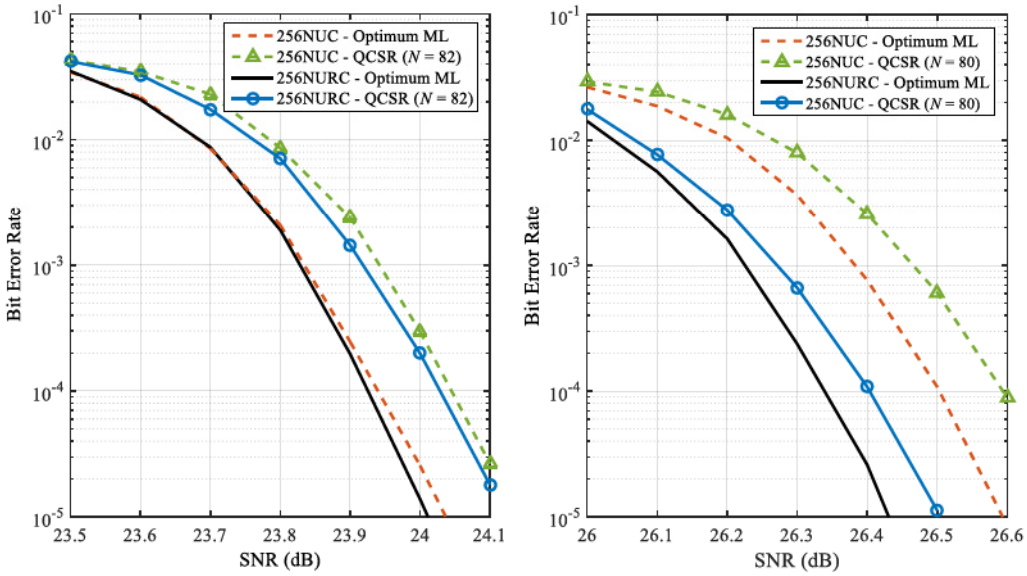


Figure 4.9: Performance comparison of ML and QCSR demappers, with and without rotation. Results presented for 256QAM and code rates 12/15 (left) and 13/15 (right), i.i.d. Rayleigh channel.

Fig. 4.9 shows the BER performance of the QCSR demapper with and without rotation, compared with the optimum ML demapper, for CRs 12/15 and 13/15. Note that only these CRs are examined, since no rotation gain is obtained for lower CRs and 256NUCs. For CR 12/15, the SNR performance of QCSR is very similar with and without rotation. However, the same does not occur with 13/15, where the SNR gain of the QCSR rotated demapper is also 0.2 dB (as the rotated ML), and the number of distances is maintained, with $N = 80$. Furthermore, compared to the non-rotated ML demapper, the QCSR rotated demapper has a 0.1 dB gain, and a complexity reduction of 69%.

4.4 Digital Quantization of LLR and I/Q Components

Quantization [67] can be defined as the procedure of constraining a continuous set of values to a discrete digital signal that can be processed, transmitted or stored in real digital processors. As reference [27] mentions, signal accuracy increases with the number of quantization bits, but high resolution signals are more costly to store and process. A low quantization resolution is hence desired for hardware implementations, since it implies a reduction of chip area, and

reduced manufacture cost and power consumption. In broadcast receivers, the highest memory requirements are always needed in the time interleaving block, since systems face signal strength fluctuations over the time, which are even higher in case of mobile reception. The memory required to store a transmit block depends on the number of quantization levels and their distribution [67]. More levels imply greater fidelity but also need more memory to store. Thus, there is a clear trade-off between in-chip memory and receiver performance.

Conventional receivers usually perform TDIL immediately before the demapping process takes place, but both operations can be swapped, minimizing memory requirements without any additional performance loss. In other words, the TDIL can be performed after the demapper, so instead of quantizing I and Q symbols, LLRs are used. Naturally, the use of NUCs affects the quantization process, since both I/Q components or LLR values after the demapper are completely different from those obtained with QAM. In this section, optimum quantizers in the sense of maximum BICM capacity are investigated. These quantizers are evaluated depending on system parameters such as receiver resolution, code rate and constellation order.

4.4.1 System Model and Considered Scenario

Following the approach given in [27], two possible receiver schemes that differ in their TDIL structure are investigated in this thesis. For the first scheme, time de-interleaving is performed directly on the I and Q components of the received signal. In this case, the components of received symbols and estimated channel gains are quantized prior to TDIL. The second scheme realizes the quantization in a different point of the receiver chain. With this architecture, demapping (the process of obtaining soft information bits from the received symbol) is performed prior to time de-interleaving. Thus, quantization is performed on the demapped LLRs, which are subsequently stored in the TDIL.

Receiver Implementation

Analog-to-digital converters in real receivers perform two fundamental operations, signal sampling and quantization. First, the continuous input signal is converted into digital with a particular sampling rate. It must fulfil the Nyquist rate-signaling criterion , with a sampling rate higher than twice the highest frequency of the input signal [85]. Afterwards, the quantizer maps the obtained sampled values to a discrete set of 2^q values, where q is the number of quantization bits or resolution [106]. The goal of the quantizer is to represent the input signal with a very small distortion, using the lowest number of q bits possible. Note that the final amount of memory in bits required to store the samples of

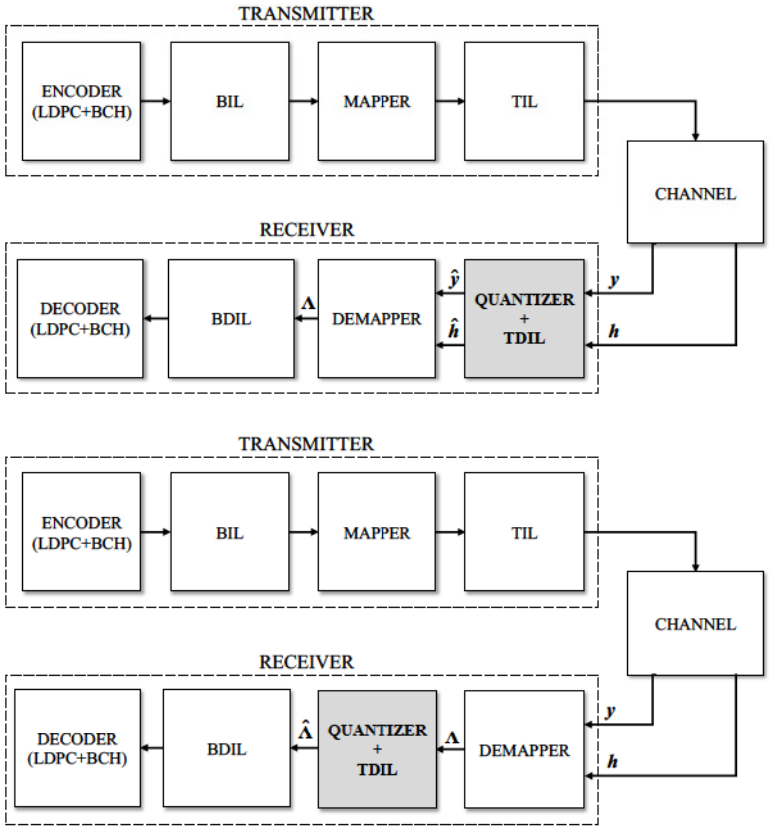


Figure 4.10: Basic diagram schemes of I/Q signal quantization (top) and LLR quantization (bottom).

the previous processing blocks directly depends on the resolution of the quantization algorithms. Fig. 4.10 shows the two different schemes considered in this thesis. At the transmitter, the constellation symbols are time-interleaved and transmitted through the channel. However, at the receiver, both schemes implement signal quantization to store received information at the TDIL memory, but at different parts of the receiving chain.

The first scheme (Fig. 4.10 top) realizes the quantization before the demapper, where received constellation symbols y and the channel estimation gains h are stored in order to perform time de-interleaving. Before storing into the time de-interleaving memory, the I and Q components of both signals are quantized. In this approach, the quantized symbols are stored prior to time de-interleaving, until the TDIL memory is filled. Afterwards, the demapper receives the quantized symbols $\hat{y}$ and quantized channel estimation gains $\hat{h}$ to calculate the corresponding LLRs. The number of LLRs calculated depend on the constella-

tion order used. The computed LLRs finally pass through the BDIL and LDPC decoder blocks, and resulting bits are used for error measurements.

The second scheme (Fig. 4.10 bottom) swaps the TDIL and demapping blocks, and therefore performs quantization in a different manner. In this case, the demapper is calculates the LLRs directly from the received constellation symbols y and channel estimates h, before the TDIL. In [69], it is shown that if the TDIL block de-interleaves groups of LLR corresponding to the received symbols and channel estimates, there is no effect in the performance. The output LLRs (Λ) at the demapper are then quantized, obtaining $\hat{\Lambda}$. Once the TDIL is filled, the groups of quantized LLRs are time de-interleaved. Finally, output LLRs pass through the BDIL and are fed to the LDPC decoder.

Uniform and Non-Uniform Quantization

A scalar quantizer can be defined as a set of disjoint intervals, $S = \{S_i; i\epsilon I\}$, where the index set I is a collection of consecutive integers beginning with 0 or 1, together with a set of reproduction values $R = \{z_i; i\epsilon I\}$. The overall quantizer is defined by $Q(x) = z_i$, for $x \in S_i$, and can be expressed as:

$$Q(x) = \sum_i z_i s_i(x) \tag{4.5}$$

where the indicator function $s(x)$ is 1 if $x\epsilon S$ and 0 otherwise. We also define $S_i = [a_i, a_{i+1}[$ as the boundaries to define each region i. The set of reproducers presented in Eq. 4.5 can be equally or non-equally spaced, considering uniform or non-uniform quantization. Note that this concept is totally different from uniform and non-uniform constellations, where the distribution refers to constellation symbols. With uniform quantization, real and imaginary parts are quantized separately and uniformly. A quantizer is said uniform when the levels z_i are equispaced. With non-uniform quantization, reproducers are no longer equispaced. An example of the possible uniform and non-uniform reproducers is shown in Chapter 2, Fig. 2.12.

Considered Scenario

Reproducer values are optimized for a DVB-NGH mobile channel model with user speed 60 km/h, since communication in motion experiences a certain Doppler shift, and TIL is performed in order to mitigate it. It is also better to transmit very robust transmission modes and hence, low-order constellations are examined, i.e. 16NUC, 64NUC and 256NUC with CRs from ATSC 3.0, from 2/15 to 13/15 with step 1/15. The simulations include inner LDPC codes with a word length size of 64800 bits. The simulated system uses 8192 sub-

carriers and a cyclic prefix of 1/4 to trade-off cell area and resilience against a 33 Hz Doppler spread in a 6 MHz bandwidth. For the performance evaluation, we transmit and decode a TIL block with $16m$ LDPC codewords, being $m = \log_2(M)$ and M the number of constellation symbols. It was confirmed with simulations that using more LDPC codewords within the TIL block does not have a significant impact on the performance. With QAM constellations, reproducers for I/Q symbols or LLRs are obtained at different SNR targets. With NUCs, the procedure is slightly different. Since each NUC is designed for a specific CR, it is necessary to calculate the LLR and I/Q reproducer values for each constellation and CR combination, already optimized for a particular SNR. The SNR in the optimization is selected as the value that provides a bit error rate (BER) of 10^{-4}, when using QAM constellations.

4.4.2 Quantization of Log-Likelihood Ratios

The proposed algorithm maximizes the BICM capacity of the system under study, which can be defined as the highest rate achievable (in the sense of asymptotically vanishing error probability) in a BICM system with independent parallel channels. It takes LLR quantized reproducers as initial inputs, and iteratively seeks the optimum capacity by changing those reproducers, making use of the Nelder-Mead algorithm [89]. The BICM capacity is calculated as the combination of capacities of all bits modulated onto a constellation symbol, using an optimum ML demapper.

From the received symbol vector y, and the channel vector h, each LLR Λ_l is computed and quantized for all code bits c_l, $l = 1, ..., m$, with m as the number of bits per constellation symbol. The expression of a single computed and quantized $\hat{\Lambda}_l$ can be denoted as follows:

$$\hat{\Lambda}_l = Q[\Lambda_l] \triangleq Q\left[\log \frac{\sum\limits_{x \in \chi_l^1} p(y|x,h)}{\sum\limits_{x \in \chi_l^0} p(y|x,h)}\right] \tag{4.6}$$

where Q denotes the quantization operation. χ_l^1 and χ_l^0 denote the complementary sets of transmit vectors for which $c_l = 1$ and $c_l = 0$ respectively. Naturally, the BICM calculation is affected since it depends on the densities of quantized symbols and LLRs $p(y|x,h)$. Rather than using a single quantizer for all LLRs, the proposed method looks for the optimum reproducer values for each bit position, modulation and CR. Depending on the constellation order, it is necessary to quantize up to m different statistics, one per each LLR. With QAM and 1D-NUC, the number can be reduced to $m/2$, since I and Q compo-

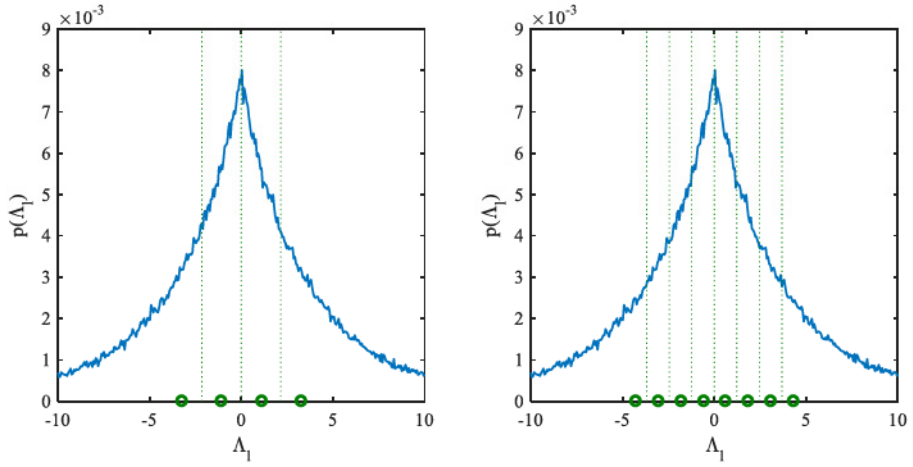


Figure 4.11: Example of probability density function and uniform quantized values of Λ_1, for a received SNR of 10 dB, 64NUC. Reproducers and boundaries are shown for 2 (left) and 3 (left) bits.

nents are repeated, and therefore odd LLRs can be replicated from even ones. However, with 2D-NUCs all LLR statistics need to be quantized separately.

Uniform Quantization

With uniform quantization, LLRs are quantized using uniform spacing of the reproducers and boundaries. Since reproducers are uniformly spaced, it is only necessary to obtain the maximum LLR quantized value of all reproducers, which simplifies drastically the optimization process. The rest of reproducers can be calculated from it.

Although the quantization does not require information about $p(\Lambda_l)$, it helps to understand the optimization and final values of quantization reproducers. Fig. 4.11 shows an example of the probability density function and uniform quantized values of Λ_1 (most significant bit) for 64NUC designed for a SNR of 10 dB, directly related to a CR 5/15. As can be observed, the higher the number of bits, the larger the maximum reproducer value. With a higher number of memory bits available, more reproducers can be used to quantize, obtaining a larger maximum value that covers better the LLR range. In this case, maximum values of approximately 3.23 and 4.30 are obtained, using 2 and 3 bits to quantize respectively. With 64NUC, the procedure has to be extended to $m = 6$ different quantizers, one per each Λ_l. For later performance results, it is only necessary to store in a look-up table (LUT) the maximum values, and the rest can be simply calculated depending on the number of bits. As an

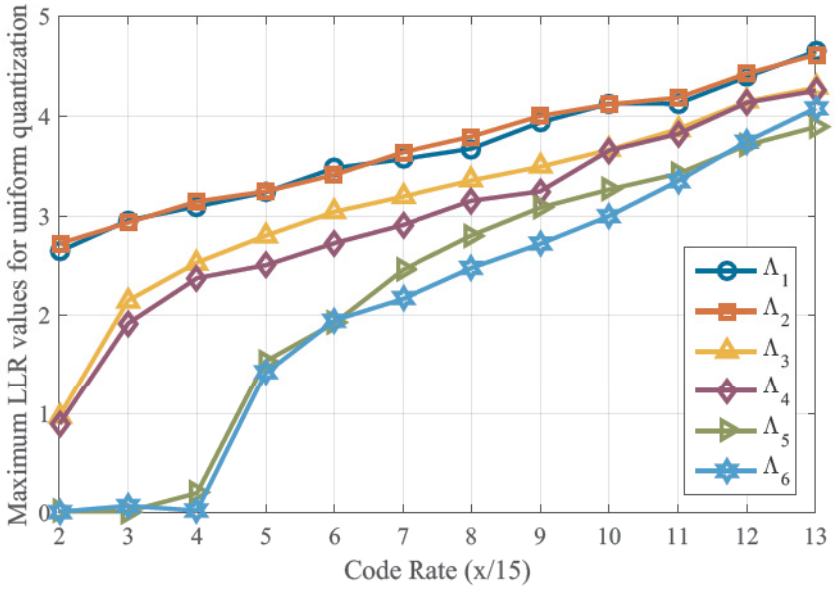


Figure 4.12: Maximum LLR reproducers, for all Λ_l. Results are shown for 64NUC, optimized for 2 bits.

example, Fig. 4.12 depicts the Λ_l maximum values for a 64NUC optimized for all CRs considered, using 2 bits per LLR.

The lower the CR used, and therefore the SNR for which the constellation is optimized, the smaller the maximum LLR reproducer. This comes from the condensation that NUCs suffer. At low SNRs, the LLR values coming from the demapper are extremely low, due to the very high noise impact. The information of the two least significant bits is forced to zero, so reproducers are close to that value. This is unique from NUCs, since QAM does not show any threshold effect for this specific bits. The very low soft-decision values indicate the LDPC a very weak reception. This clearly has an impact in the number of bits required. On the other hand, the quantized values for the most significant LLRs are high, due to the larger distance between symbols with the same bit in the I/Q space.

Non-Uniform Quantization

With non-uniform quantization, the optimum reproducers are also obtained through an algorithm that maximizes the BICM capacity. Unlike uniform quantization, all positive reproducer values need to be optimized separately. Due to the left-right and up-down symmetry of NUCs, negative reproducers can be derived from positive ones. Therefore, the number of reproducers to

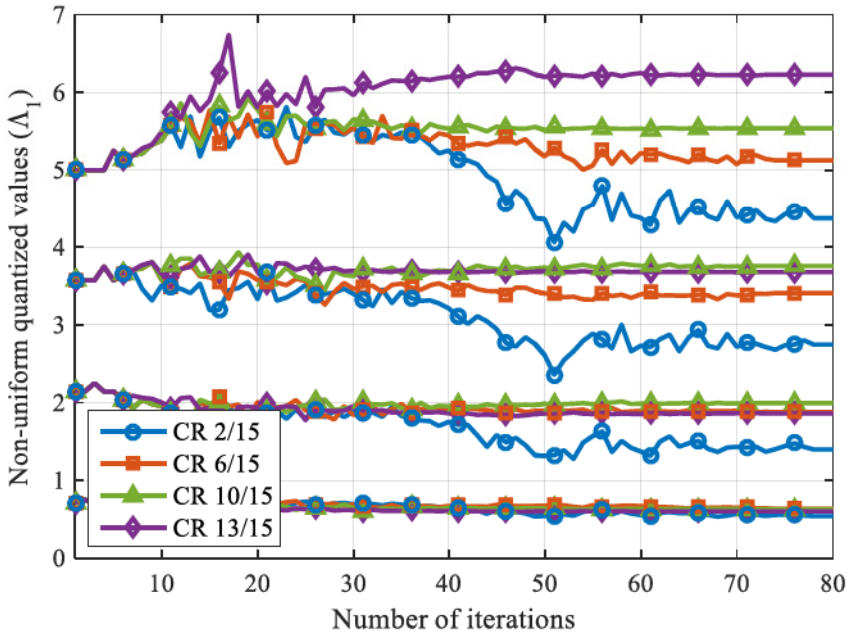


Figure 4.13: Λ_1 quantized values with recursive non-uniform optimization, for different 64NUCs optimized for CRs 2/15, 6/15, 10/15 and 13/15. 3 quantization bits, i.e. 4 positive levels.

optimize is 2^{q-1}, being q the number of quantization bits selected. As expected, more degrees of freedom are directly related with a better performance, since the capacity can be further optimized, which can be translated into less TDIL memory required at the receiver.

Fig. 4.13 depicts an example of a non-uniform optimization process, using the algorithm defined in [89]. Reproducer values are shown for different iterations and a quantized Λ_1, using 3 bits, which means that 4 positive reproducers are optimized. The optimization is shown for 4 different 64NUCs, designed for CRs 2/15, 6/15, 10/15 and 13/15. Initial values are taken from uniform quantization. The optimized reproducers change differently depending on the shape of the constellation and SNR. Optimized reproducers are uniform-like when using low CRs. A different situation is obtained with high CRs, where strongly non-equispaced reproducer values are obtained.

4.4.3 Quantization of I/Q Components

For the scheme considered in Fig. 4.10 (top), the signals y and h need to be quantized. As with LLRs, 2^q-level scalar quantizers are considered. In this case, quantizers do not depend on the code bit position. I and Q components

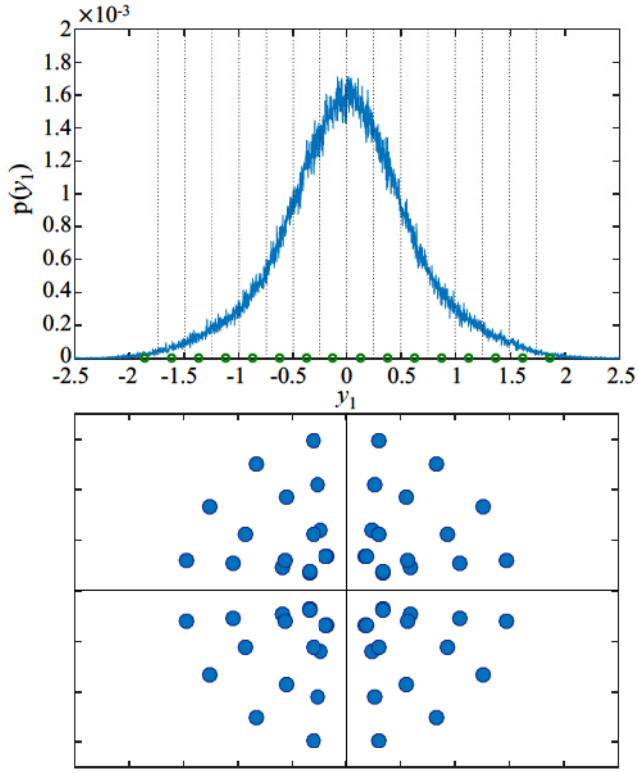


Figure 4.14: Probability density function and uniform quantized values of the I component with 4 bits, for a received SNR of 11 dB (CR 6/15). The corresponding 64NUC used is also shown.

of received symbols y and channel estimates h are quantized independently. In this case:

$$\Lambda_l \triangleq \log \frac{\sum\limits_{x \in \chi_l^1} p(\hat{y}|x, \hat{h})}{\sum\limits_{x \in \chi_l^0} p(\hat{y}|x, \hat{h})} \tag{4.7}$$

where $\hat{y} = Q_1[y]$ and $\hat{h} = Q_2[h]$ are the quantized receive signal and channel coefficient, respectively, and $p(\cdot)$ refers to the conditional probability density function of $\hat{y}$ given x, $\hat{h}$. Naturally, the BICM calculation is affected since it depends on the densities of quantized symbols and LLRs. It should be noted that received symbols and channel estimates are quantized in a different manner. While receive signal components need different reproducers for each NUC and CR combination, channel estimates require only one quantizer design, since they are independent from the SNR.

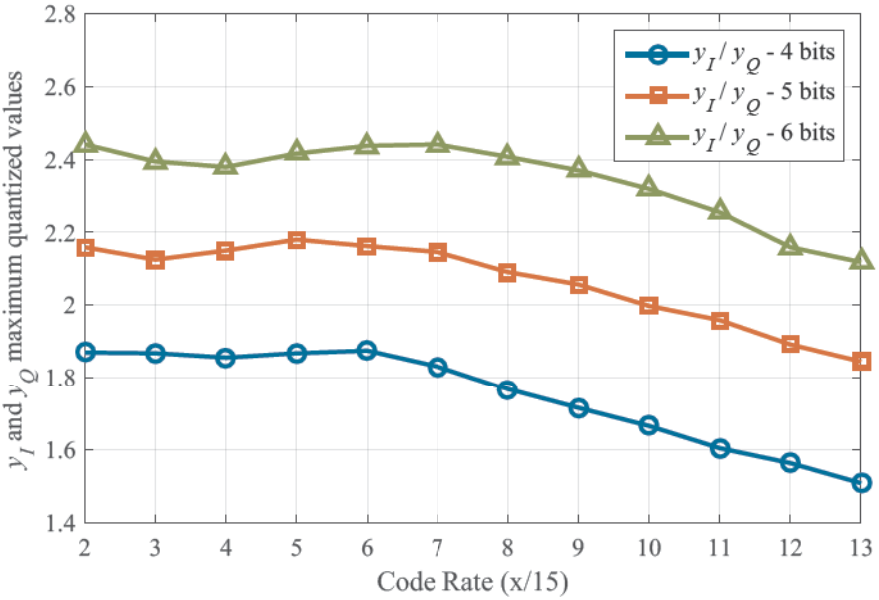


Figure 4.15: Maximum quantized values of I and Q components (y_I and y_Q). Results are shown for 64NUC, quantized using 4, 5 and 6 bits.

Uniform Quantization

In this section, y and h are quantized using a uniform spacing of reproducers and boundaries. As with LLRs, it is only necessary to obtain the maximum quantized reproducer. The rest of reproducers can be calculated from it. Fig. 4.14 shows an example of the probability density function and uniform reproducers with 4 bits of the I component of y. The corresponding 64NUC used is also shown in Fig. 4.14. The constellation was designed for a SNR of 11 dB, which is related to CR 6/15. Similar values are obtained for the Q component. When I and Q components are quantized, more bits are required compared to LLRs, in order to obtain similar BICM capacities. However, only 4 components need to be quantized, which is a potential advantage when using high-orders of constellation. Maximum reproducer values of 1.86, 2.17 and 2.43 are obtained for the I component, using 4, 5 and 6 bits respectively.

The quantizer parameters for the receive signal have to be designed and stored for all CR combinations. In contrast, the quantizers for the channel coefficients need to be designed and stored only once. Fig. 4.15 shows the maximum reproducers of I and Q components for the received signal y, with a 64NUC and the considered channel model. I and Q quantizers are identical, due to symmetry. With NUCs, large maximum quantized values are required for low CRs. At low SNRs, the very high noise impact affects the received

symbol, requiring higher reproducers. However, slightly lower values are needed with NUCs, due to the condensation. Regarding the channel estimates, the maximum reproducer values are 1.33, 1.54 and 1.73 for both components, using 4, 5 and 6 bits respectively. As mentioned above, these reproducers do not depend on the constellation shape and SNR. Note that these values may vary, if different channel conditions are selected.

Non-Uniform Quantization

With non-uniform quantization, all positive reproducers are optimized separately. Due to the symmetry of quantized symbols, all negative reproducers can be derived from positive ones. Therefore, the degrees of freedom are again 2^{q-1}. Compared to uniform quantization, the most significant improvement in terms of BICM capacity is achieved using high CRs. In next sections, we also analyze the performance of non-uniform quantization of I and Q components.

4.5 Quantization Loss vs. Time De-Interleaving Memory Trade-Off

In this section, ATSC 3.0 physical layer simulation results are provided to illustrate the performance achieved with LLR and I/Q quantization for different constellations and CR combinations, and different quantizer resolutions. ML demapping is used. To provide reliable results, the performance is evaluated under different channel realizations for each SNR, i.e., different seeds for the (pseudo) random generators for each SNR. For a given SNR, all receiver configurations are simulated under the same set of channel realizations. For each SNR a maximum number of 10^4 and a minimum number of 10^3 TIL blocks are considered. The simulation is stopped when 100 erroneous TIL blocks are detected. A TIL block is considered erroneous when an erroneous bit is detected in the entire TIL block. Finally, the selected quality of service for comparisons is a bit error rate (BER) of 10^{-4} after BCH (Bose-Chaudhuri-Hochquenghem) decoding.

4.5.1 Performance Loss of LLR Quantization

This subsection evaluates the performance achieved with LLR quantization in the considered scenario, using the reproducers saved in the LUT. For the sake of simplicity, we show results using 64NUCs, but the complete process is extended to 16NUCs and 256NUCs. In Fig. 4.16, the particular case of CR 13/15 is shown, since it is the least robust mode, and more bits are required to

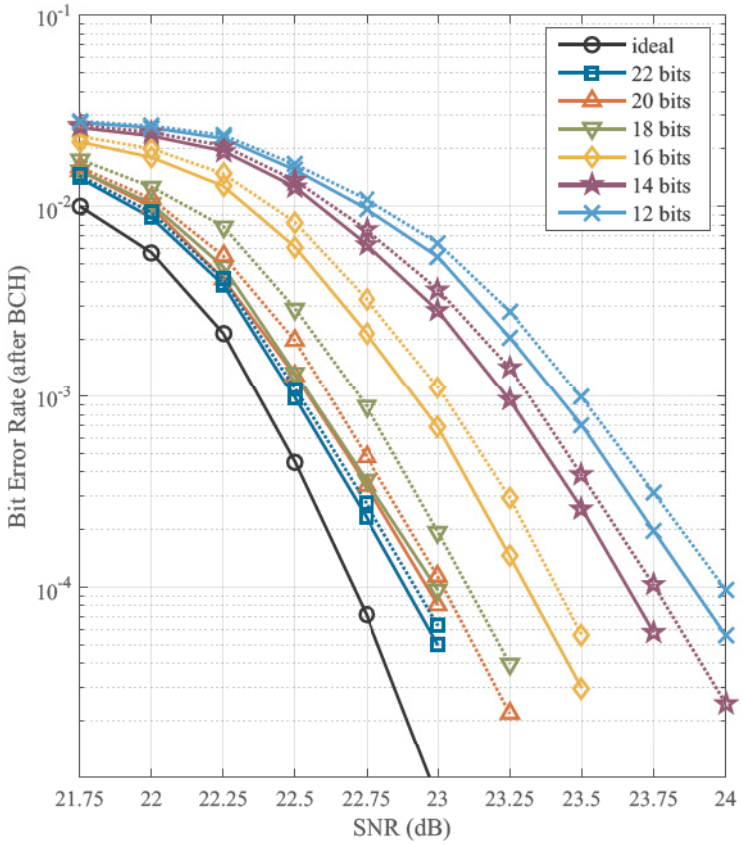


Figure 4.16: Performance evaluation of uniform (dashed lines) and non-uniform (continuous lines) LLR quantization, using 12 to 22 bits and compared to the non-quantized optimum performance, for 64NUC and CR 13/15.

Quantization bits	**12**	**14**	**16**	**18**	**20**	**22**
$\Lambda_1 = \Lambda_2$	3	3	3	4	4	4
$\Lambda_3 = \Lambda_4$	2	2	3	3	3	4
$\Lambda_5 = \Lambda_6$	1	2	2	2	3	3

Table 4.4: Number of bits per LLR for 64NUCs, depending on the total number of bits available.

quantize. The optimum non-quantized performance (black line) is compared with uniform (dashed lines) and non-uniform (continuous lines) quantization methods. In particular, the BER achieved with LLR quantization with several illustrative combinations is studied, i.e. different number of bits are used for each LLR, depending on the maximum reproducer obtained. Combinations of 2, 3 and 4 bits for each received LLR are considered, as shown in Table 4.4.

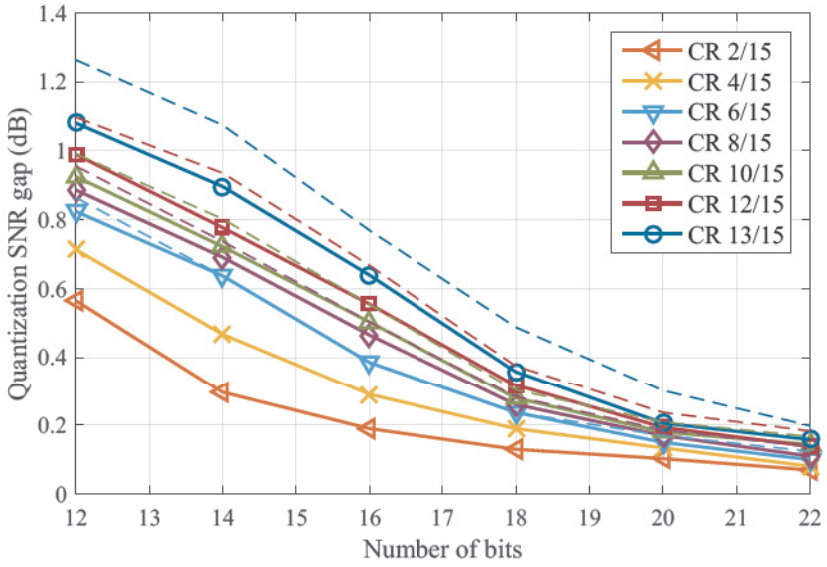


Figure 4.17: SNR gap of uniform (dashed lines) and non-uniform (continuous lines) LLR quantized 64NUCs, using 12 to 22 bits.

	CR (x/15)	2	4	6	8	10	12	13
Uniform	**16NUC**	10	11	12	12	12	13	14
	64NUC	15	17	18	19	19	20	21
	256NUC	21	23	24	25	26	28	30
Non-Uniform	**16NUC**	10	11	11	12	12	12	13
	64NUC	15	17	18	18	18	19	20
	256NUC	21	22	23	24	25	26	28

Table 4.5: Minimum number of uniform and non-uniform LLR quantization bits. SNR gap below 0.25 dB.

As expected, the larger the number of bits the better the performance. Moreover, the difference between uniform and non-uniform quantization becomes almost negligible when using more bits, due to performance obtained, close to the optimum. Fig. 4.17 shows the SNR gap relative to the non-quantized case for a BER = 10^{-4}, for all considered 64NUC and CR combinations. Non-uniform is always at least as good as uniform, with real gains at high CRs. For practical purposes, we postulate 0.25 dB as the maximum tolerable degradation due to quantization. This is a suitable value since the DVB-NGH channel model with speed 60 km/h is used.

It is possible to provide a concrete number of bits $Q = \sum_{l=1}^{L} q_l$, with L as the number of elements, to quantize each NUC and CR combination. The same

Quantization bits	16	18	20	22	24	26	28	30
$y_1 = y_2$	4	5	6	6	7	7	8	8
$h_1 = h_2$	4	4	4	5	5	6	6	7

Table 4.6: Number of bits per I/Q component for 64NUCs, depending on the total number of bits available.

procedure can be performed to 16NUC and 256NUC constellations. Table 4.5 summarizes the necessary number of bits q for some representative CRs: 2/15, 4/15, 6/15, 10/15, 12/15 and 13/15, considering both uniform and non-uniform quantization. One can affirm that Q/m is almost independent of the constellation, e.g. $Q/m = 3$ for non-uniform quantization of all NUCs at CR 8/15. This means that the number of quantizer bits per code bit is constellation-invariant and varies only little with CR. Note that when a odd number of bits is selected, the assignment is done as shown in Table 4.4, with 1 bit of resolution subtracted from the least significant LLR.

4.5.2 Performance Loss of I/Q Components Quantization

In this section, the performance achieved with I/Q quantization is evaluated. Results are shown for 64NUC constellations, but the complete process has been repeated using 16NUCs and 256NUCs. Fig. 4.18 shows the performance obtained for all NUC and CR combinations. Combinations of 4, 5, 6, 7 and 8 bits for each received real component are considered, as shown in Table 4.6.

With I/Q components, the number of bits used influences drastically the overall performance. Using 64NUCs designed for low CRs, just a low number of bits is required to quantize all signal components with a negligible SNR gap, due to strong and robust CR applied after the demapping process. However, using high CRs and keeping the same number of bits decreases the overall performance. Another interesting point is that non-uniform quantization always needs same or fewer bits to achieve the target performance. The same procedure can be extrapolated to 16NUC and 256NUC constellations. Table 4.7 summarizes the necessary number of bits $Q = \sum_{l=1}^{L} q_l$ for some representative CRs: 2/15, 4/15, 6/15, 10/15, 12/15 and 13/15, considering both uniform and non-uniform quantization. Comparing these results and results from Table 4.5, I/Q quantization is worse than LLR quantization, except for 256NUC at CR 2/15, 4/15 and 6/15. For this reason, only LLR quantizers are considered in next section.

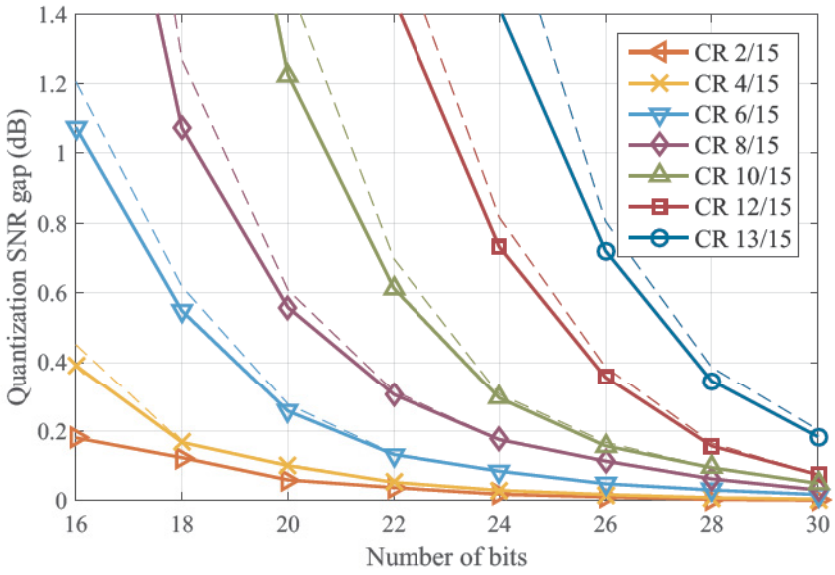


Figure 4.18: SNR gap of uniform (dashed lines) and non-uniform (continuous lines) I/Q quantized 64NUCs, using 16 to 30 bits.

	CR (x/15)	2	4	6	8	10	12	13
Uniform	**16NUC**	14	16	18	19	21	23	25
	64NUC	15	17	20	23	25	27	30
	256NUC	17	19	22	25	28	31	34
Non-Uniform	**16NUC**	14	16	18	19	21	22	24
	64NUC	15	17	20	23	25	27	30
	256NUC	17	19	22	25	28	30	33

Table 4.7: Minimum number of uniform and non-uniform I/Q quantization bits. SNR gap below 0.25 dB.

4.5.3 Time De-Interleaving Memory Requirements

The total amount of memory needed at the TDIL, Δ, can be calculated as expressed in Eq. 2.32, already introduced in Chapter 2, Section 2.3.2. In ATSC 3.0, maximum interleaving depths of $\Gamma = 2^{19}$ for NUCs can be transmitted. Since Γ is fixed, a reduction of Δ is in one-to-one correspondence to a reduction of Q, selected in previous sections.

Practical receivers use 6 bits per LLR [107], and 10 bits per I/Q component [28] in TDIL quantization. The total amount of memory used as reference when quantizing LLRs is 12.58, 18.87 and 25.17 Mbits for 16NUC, 64NUC and 256NUC respectively, while 20.97 Mbits are required with I/Q components in all cases. For instance, from results presented in previous sections we can affirm

	Code Rate	TDIL Memory (Mbits)	Reduction (%)
16NUC	2/15	5.242	58.3
	4/15	5.762	54.2
	6/15	5.762	54.2
	8/15	6.291	50
	10/15	6.291	50
	12/15	6.291	50
	13/15	6.816	45.8
64NUC	2/15	7.864	58.3
	4/15	8.913	52.7
	6/15	9.437	50
	8/15	9.437	50
	10/15	9.437	50
	12/15	9.961	47.2
	13/15	9.961	47.2
256NUC	2/15	8.913	57.5
	4/15	9.961	52.5
	6/15	11.534	45
	8/15	13.107	37.5
	10/15	13.107	37.5
	12/15	13.631	35
	13/15	14.681	30

Table 4.8: Summary of required memory and reduction percentage with LLR quantization for all combinations considered.

that a 16NUC optimized for a CR 13/15 needs 13 bits to quantize all LLRs, as shown in Table 4.5. In this case, $\Delta = 2^{19} \times 13$ bits, i.e. 6.81 Mbits are required, and compared to the 12.58 Mbits value, a 45.8% reduction of in-chip memory is achieved.

Comparing the results obtained in Table 4.5, and using Eq. 2.32, it is possible to determine the in-chip memory reduction, relative to the lowest quantization memory of reference (12.58, 18.87 and 20.97 Mbits for 16NUC, 64NUC and 256NUC respectively). Table 4.8 depicts the memory Δ required, and the reduction percentage achieved for each modulation and CR considered. Note that non-uniform quantization is always used, since it always provides same or better results than uniform. The higher the CR and modulation used the lower the reduction achieved. A reduction from 30% to 58.3%, depending on the combination used, is obtained.

4.6 Conclusion

In this chapter, the impact of NUCs on real receivers has been investigated from two different points, i.e. demapping of constellation symbols and quantization of I/Q components or LLR values obtained. Different algorithms have been also proposed as possible solutions to minimize the problems detected.

For the first case considered, a complete analysis on demapping complexity has been provided. The number of distances to calculate with QAM and 1D-NUCs can be drastically reduced by using a 1D-demapper, as proposed in [26], and explained in Chapter 2. However, with 2D-NUCs and RCs , the demapper has to evaluate all distances in two dimensions. To reduce this complexity, a suboptimum demapper called QCSR has been proposed. The demapper is based on the combination of two strategies to take advantage of the symmetry of the constellations and the condensation, i.e., similar I/Q values of several constellation symbols, of NUCs at low SNRs. An example of application has been shown for 2D-256NUCs. A reduction in the number of required operations from 69% to 93% has been achieved, depending on the CR, when compared to the optimum ML demapper, with almost no performance degradation (under 0.1 dB). The demapper can be extrapolated to the different orders of constellation considered in this thesis, i.e. 2D-16NUC and 2D-64NUC, or even larger constellations such as 2D-1kNUC or 2D-4kNUC. It can be applied to rotated constellations as well, without any complexity or performance implication.

The influence of NUCs on digital quantizers has been also studied. A different shape implies different distributions for the I/Q components and the LLRs obtained after the demapping process. To reduce the amount of bits to store at the TDIL, a new strategy based on BICM capacity maximization via the Nelder-Mead algorithm has been proposed. It has been applied to both I/Q components and LLR values, selecting the best case for each modulation and CR combination, and providing memory reduction percentages compared to conventional quantizers. In general, non-uniform LLR quantization is the best choice in the sense of meeting the performance target with minimum memory requirements. The use of non-uniform quantizers adapted to the signal statistics provide slight improvements in terms of performance or alternatively in-chip memory savings. For the worst case considered, i.e. 256NUC with CR 13/15, a final reduction in TDIL memory of 30% compared to conventional quantizers has been achieved, when quantizing LLR values. Better results have been obtained for low-order constellations. With 16NUCs, the total memory reduction ranges from 45.8% to 58.3%. For 64NUCs, reduction percentages from 47.2% to 58.3% have been also obtained.

Chapter 5

Non-Uniform Constellations for MIMO Communications

The use of non-uniform constellations in single-antenna broadcast communications has been studied in Chapters 3 and 4 from different transmit and receive points of view, respectively. This includes the optimization process, performance analysis and complexity (demapping and quantization). With MIMO, both transmit and receive systems are modified, since multiple antennas are used. The use of several antennas clearly affects both the channel model and the SNR range in which the constellations work. Constellations optimized for SISO may not be optimum for MIMO, as proposed in the ATSC 3.0 standardization process. In addition, further parameters need to be considered: power imbalance (PI), cross-polar discrimination (XPD), number of transmit and receive antennas, or correlation factor. In this thesis, two transmit and receive cross-polar antennas are assumed. The influence of these parameters as well as the difference between SISO and MIMO configurations is studied in Sections 5.1 and 5.2.

At the receiver, one of the most important drawbacks is the extremely high demapping complexity when using NUCs and optimum ML or max-log demappers. Section 5.3 provides a complete demapping complexity analysis, which shows that the number of possible received symbols grows exponentially with the number of antennas and the constellation order. To reduce this complexity, different sub-optimum demappers can be used. In Section 5.4, the particular case of the SFSD demapper is analyzed. It entails a good trade-off between

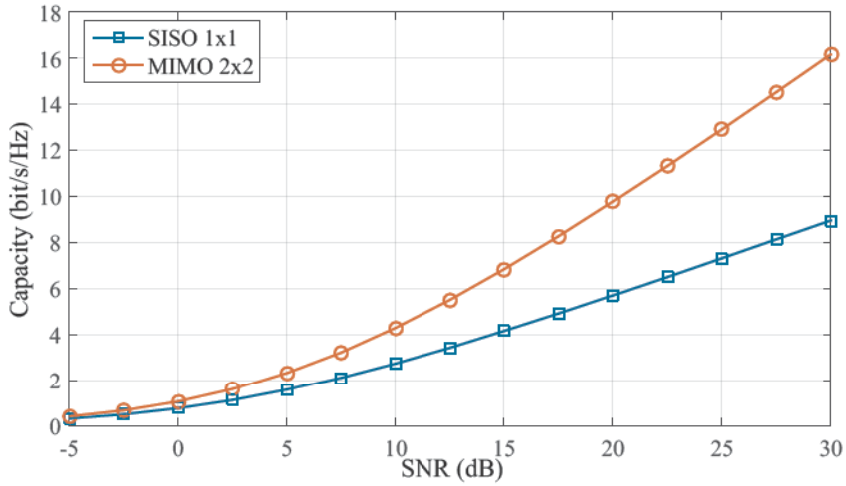


Figure 5.1: Ergodic capacity for a mobile DVB-NGH channel model, with user speed 60 km/h, and same transmit power in the two cases.

performance and demapping complexity. With SFSD, it is necessary to perform a quantization step that needs to be performed in separated I and Q components [80]. Thanks to the squared shape of QAM and 1D-NUCs, both components can be separated. However, this is not possible with 2D-NUCs. In this chapter, and an efficient pre-processing approach for 2D-NUCs based on the Voronoi regions for the quantization step is proposed.

5.1 Multi-Antenna Non-Uniform Constellations

The implementation of MIMO provides three different types of gains: array gain, diversity gain, and multiplexing gain [75]. The array gain comes from the coherent combination of the received signals from the multiple antennas. For co-polar antennas, this gain equals 3 dB every time the number of antennas is doubled. The diversity gain is due to the fact of having several spatial branches with independent fading between the transmitter and receiver. And the multiplexing gain allows transmitting more than one data stream [76]. Fig. 5.1 shows the ergodic capacity for SISO and MIMO with two transmit and two receive antennas, in the mobile DVB-NGH channel (user speed 60 km/h) [33].

The MIMO capacity increases with the SNR at a higher rate than the SISO scheme. This difference in spectral efficiency is due to multiplexing gain for a MIMO channel employing two transmit and receive antennas with independent streams. The gain depends also on the particular channel. For the analyzed case, increased diversity due to multiple antennas at low SNR levels provides

very significant gains in relative terms. The DVB-NGH mobile model gives a capacity gain (vertical axis) compared to SISO of 40%, 48% and 57%, for 0, 5 and 10 dB SNR, respectively. Fig. 5.1 also depicts the difference in SNR between the two configurations utilized. For instance, in order to achieve a channel capacity of 4 bit/s/Hz, and using just a single antenna in both transmit and receive sides, a minimum SNR of approximately 15 dB is necessary. With 2×2 MIMO systems, the SNR required is reduced to 10 dB. Therefore, there is a difference in performance of 5 dB between both configurations. This difference logically influences the optimization process, since the SNR target for which the NUC is designed totally changes. However, not only the use of two receive and transmit antennas modifies the constellation shape. As already mentioned, more parameters may change the final result when optimizing NUCs for MIMO. Capacity and performance gains over QAM obtained need to be analyzed and compared with those obtained in SISO as well.

In this section, we follow a similar structure than Section 3.2 in Chapter 3. Two different optimization techniques are investigated and particularized for MIMO, depending on the number of real-valued dimensions considered in the optimization process: 1D- and 2D-NUCs. Since constellations optimized in this chapter are compared with those optimized for SISO in Chapter 3, it is necessary to differentiate them with a new notation. A constellation optimized for 2×2 MIMO configurations is called in this dissertation Multi-Antenna Non-Uniform Constellation (MA-NUC). Constellations optimized for one and two dimensions are then called 1D-MA-NUC and 2D-MA-NUC, respectively. On the other hand, constellations optimized for SISO but used in MIMO are referred just as 1D-NUC and 2D-NUC. The optimization process of both 1D-MA-NUC and 2D-MA-NUC is explained in following subsections.

5.1.1 Preliminary Design

In this section, we investigate in detail the concrete parameters that affect the optimization process by the use of two transmit and receive antennas. In particular, three different subsections are considered. First, the optimization of NUCs in one or two antennas is analyzed. The first option maximizes the mutual information in a single antenna, optimizing the constellation transmitted in the first antenna and replicating the same result in the second antenna. The second option optimizes both constellations independently, achieving better capacity results at the expense of a higher optimization complexity. This becomes especially effective when considering a PI between antennas, where a different SNR is required in each antenna. The second subsection studies the demapping influence on constellations, and selects the best option in terms of performance and complexity. Finally, several channel models are analyzed.

Optimization in 1 or 2 Antennas

Traditional 2×2 MIMO systems that use a symmetric modulation in both transmit antennas utilize $2\log_2(M)$ bits per cell, where M is the number of symbols in a single antenna. In such case, and using uniform QAM constellations, the half of the bits is transmitted in one antenna, while the other half is used in the other, using identical constellations in both of them. For example, 12 bits per cell means that 6 bits are associated to each antenna, where 64 symbols are used.

Considering no power imbalance between antennas, one could think that such symmetry must be maintained with MA-NUCs. However, the optimization process allows us to explore new possibilities. The first option is simply to optimize the constellation transmitted in the first antenna, replicating and transmitting it in the second antenna as well. The parameters to configure are still grouped in a single vector $\mathbf{a} = [a_1, a_2, ..., a_N]$, with N as the degrees of freedom in the optimization, which depends on the constellation order. Compared to SISO, the optimization burden is maintained. The second option is to optimize both constellations by separate, identifying two different and independent vectors:

$$\begin{cases} \mathbf{a_1} = [a_{11}, a_{12}, ..., a_{1N}] \\ \mathbf{a_2} = [a_{21}, a_{22}, ..., a_{2N}] \end{cases} \tag{5.1}$$

where the first index indicates the transmit antenna, and the second term represents the position of the constellation symbol under study. In this section, an i.i.d. Rice channel with $K = 10$ (as defined in Appendix A) is considered, since it is a model used for cross-polarized MIMO with fixed rooftop reception and LoS. The main idea is to observe the similarities and differences introduced by the channel to the two optimization options already considered, but also to take into account the new parameters that influence the process such as PI or XPD. Fig. 5.2 shows the evolution of the two parameters a_{11} and a_{21} when optimizing each 1D-MA-16NUC constellation independently for a SNR of 20 dB, without PI. Three different XPD values are also evaluated: 0, 6 and ∞ dB.

As Fig. 5.2 shows, both a_{11} and a_{21} parameters evolve towards the same (or almost) final value, regardless of the cross-polar discrimination introduced. The XPD at the receiver can be calculated as [108]:

$$\text{XPD}_1 = \frac{|h_{11}|^2}{|h_{21}|^2} \tag{5.2}$$

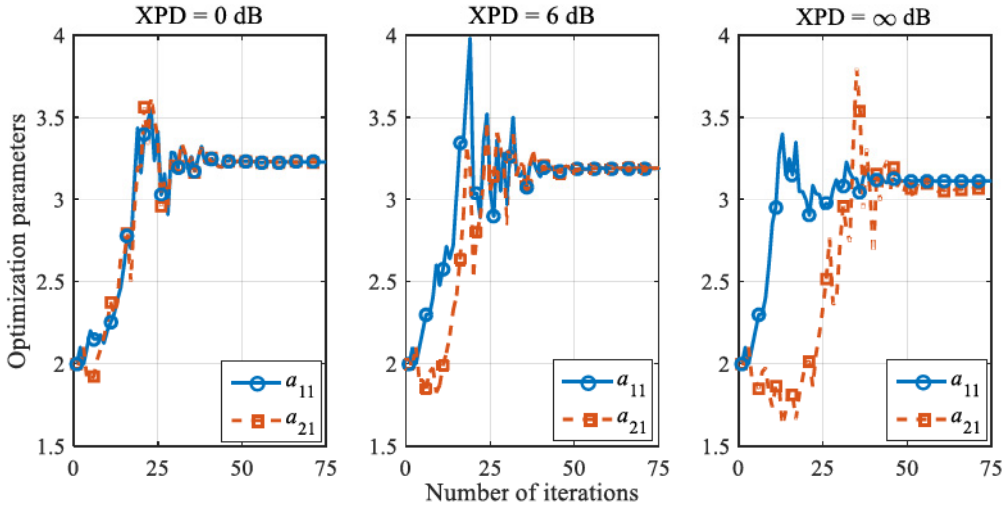


Figure 5.2: Evolution of the optimization parameters a_{11} and a_{21}, for 16-MA-NUCs, SNR 20 dB and three different XPD values: 0, 6 and ∞ dB.

$$\mathrm{XPD}_2 = \frac{|h_{22}|^2}{|h_{12}|^2} \tag{5.3}$$

The term XPD_1 denotes the average power of the co-polar term (direct path) for the first antenna divided by the average power of the cross-polar term, introduced to the incorrect reception antenna, in this case the second one. In addition, both terms need to fulfill that $\sum_i^2 |h_{i,j}|^2 = 1$. Note that the channel is symmetrically generated:

$$\mathrm{XPD}_1 = \mathrm{XPD}_2 \tag{5.4}$$

Thus, an XPD = 6dB = 4 (lineal scale) determines a channel matrix in which the co-polar terms are transmitted with average power $|h_{11}|^2 = |h_{22}|^2 = 0.8$, and cross-polar terms with $|h_{21}|^2 = |h_{12}|^2 = \frac{0.8}{4} = 0.2$. For the extreme case where XPD = 0dB = 1 (lineal scale), all terms have average power 0.5. On the other hand, with XPD = ∞, both cross-polar terms are zero, while direct paths $|h_{11}|^2 = |h_{22}|^2 = 1$. For this reason, optimized values in Fig. 5.2 are very similar for both antennas, due to the expression 5.4. Without PI, both constellations tend towards the same final result, since received signals in the two receive antennas have on average the same power. The XPD value also affects the optimized parameters obtained. Larger XPD values affect less the two signals at the receive antennas, requiring symbol positions as uniform as possible (they tend to uniform QAM).

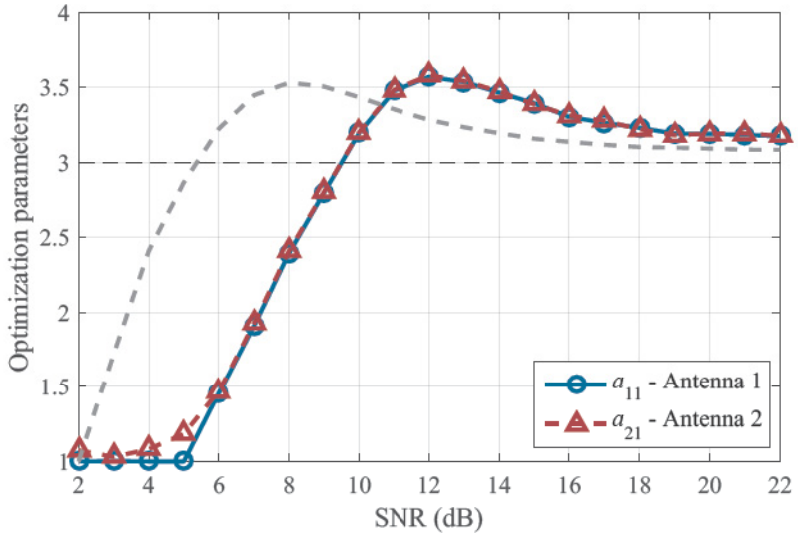


Figure 5.3: Optimization parameters a_{11} and a_{21} for 1D-MA-16NUCs as a function of the SNR, i.i.d. Rice channel with $K = 10$.

Fig. 5.3 shows the whole SNR range for the 1D-MA-16NUCs considered in the two different antennas, for i.i.d. Rice channel and XPD = 6 dB. Based on these results, from now it is assumed $\mathbf{a_1} = \mathbf{a_2} = \mathbf{a}$ for PI = 0 dB, i.e. the same constellation is used in both antennas. This assumption logically cannot be taken when using PI. Fig. 5.3 also shows the difference between SISO and MIMO. There is a clear shift in SNR between both results, mainly because of the 3 dB coming from the array gain and the cross-polarized terms at the receiver. The fact that constellations adapt dynamically to the number of antennas and XPD means that NUCs optimized for SISO can be used for MIMO as well, and vice versa. NUCs that are designed for SISO and for a specific modulation and CR combination can still be used for MIMO, for the same configuration. This assumption was already taken in the ATSC 3.0 specification [76], and will be proved in Section 5.2, where performance results are provided.

Influence of ML, ZF and MMSE Demappers

In this section, we study the influence of the type of demapper used on the optimized NUCs. Although the ML demapper obtains optimum performance, it entails a high demapping complexity that increases with the order of constellation and number of antennas. In this sense, several equalization methods such as ZF or MMSE can be used to reduce the complexity. The use of these

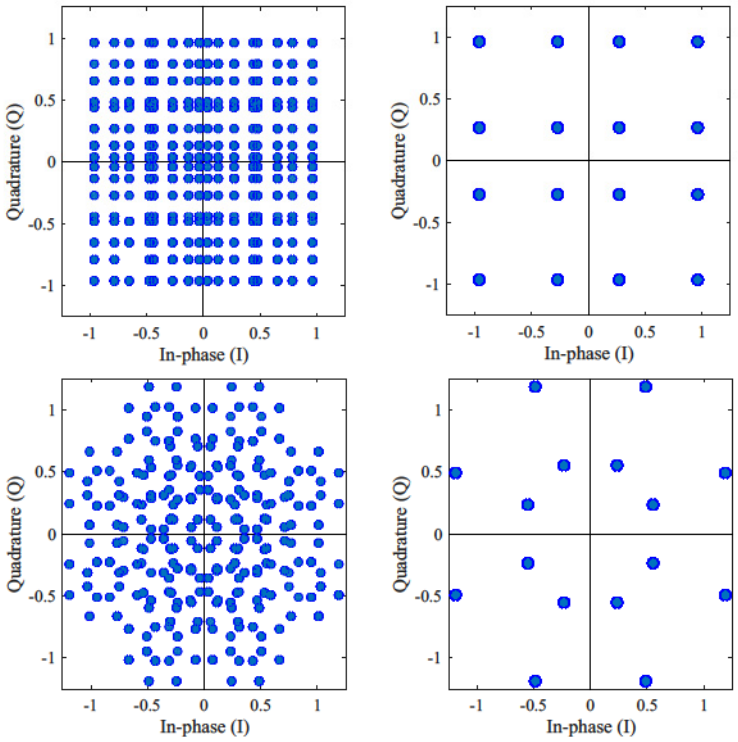


Figure 5.4: Examples of 1D- and 2D-16NUCs at the receiver input, before (left) and after (right) equalization, noise-free reception.

equalizers reduces enormously the demapping complexity, accelerating the optimization process and allowing to optimize very high-order constellations (ML with MIMO is not computationally feasible from 1kNUC on). In fact, many real receivers implement this technology to facilitate real-time demodulation. Note that sphere decoders can be used as well to reduce complexity. However, they are not considered in this section since their use is not straightforward. SD is explained in Section 5.4.

The demapping schemes considered when using MMSE and ZF equalizers can be found in Chapter 2. An optimum ML demapper computes LLRs for all code bits $2B$, where B refers to the number of bits per symbol used in a single antenna. For the LLR computation, a total number of M^2 Euclidean distances between the received vector $\mathbf{y}$ and constellation symbols $\mathbf{x}$ is calculated. The received constellations in the two antennas present the following expression:

$$\begin{cases} y_1 = h_{11}x_1 + h_{12}x_2 \\ y_2 = h_{21}x_1 + h_{22}x_2 \end{cases} \tag{5.5}$$

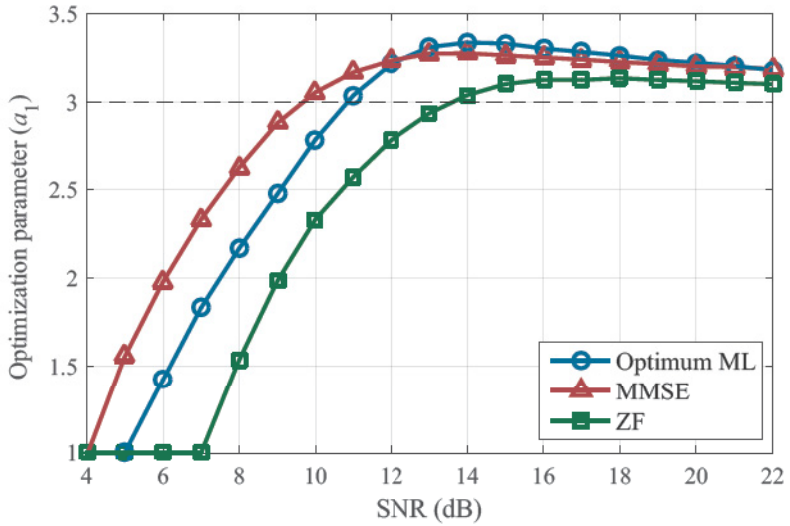


Figure 5.5: Optimization parameter a_1 for 1D-MA-16NUCs and different MIMO demappers, i.i.d. Rayleigh channel. Results are also compared to SISO.

As a consequence, the received constellation in each antenna is a linear combination of both x_1 and x_2, which depends on the XPD introduced. On the other hand, ZF and MMSE linear equalizers transform the joint MIMO demapping process into independent single-antenna demapping blocks. In a 2×2 MIMO system, the ML demapper with complexity M^2 is transformed into two independent ML demappers with complexity M. To do this, the cross components of the channel (h_{12}, h_{21}) are suppressed, providing two estimates $\tilde{y}_1$ and $\tilde{y}_2$ of the received symbol. LLRs are then calculated and combined in a single stream. Fig. 5.4 shows an example of 1D- and 2D-NUCs at the receiver input for the first antenna, before (left) and after (right) equalization with MMSE. Noise-free reception is assumed to better show the resulting constellations, where $\mathbf{H} = \mathbf{I}$ and XPD = 6 dB.

Naturally, the use of linear equalizers distorts the received signal, which turns into slightly different optimization values. Fig. 5.5 shows the a_1 value optimized for a 1D-MA-16NUC and a complete SNR range, for the different demappers considered above. It is assumed that the same constellation is transmitted over the two antennas. When ZF is used, the receive signal is equalized making use of the channel matrix, not considering the noise introduced, as expressed in Eq. 2.29, in Chapter 2. As a consequence, the noise is amplified, which transforms the optimized constellation into a more condensed one with lower a_1 value. A different behavior can be seen when using MMSE. In this case, the noise power is included, making the a_1 value more similar to ML,

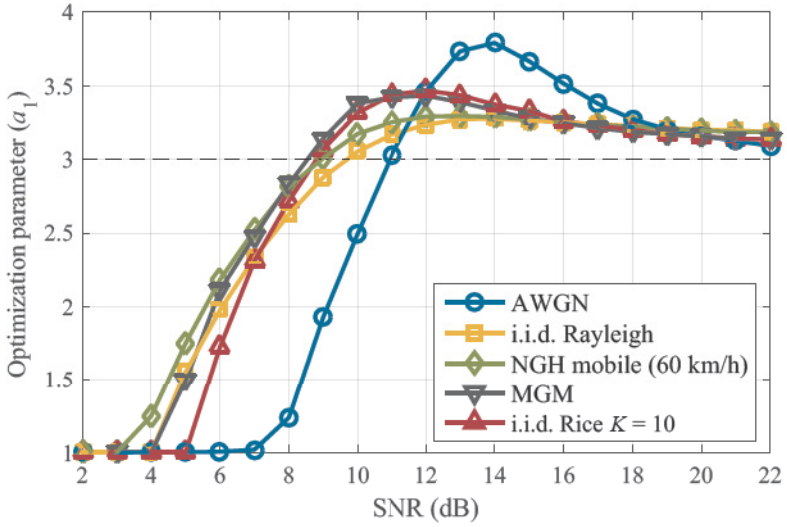


Figure 5.6: Optimization parameter a_1 for 1D-MA-16NUCs and different channel models: AWGN, i.i.d. Rice, mobile DVB-NGH and MGM.

especially at high SNRs where this type of equalizer works better. On average, the difference between ML and ZF in the final optimization parameter, for the whole considered SNR range, is 0.23 (distance in a single component), while the difference between ML and MMSE is reduced to 0.11. From this point, we assume an MMSE equalizer for this section.

Selection of Channel Model

As already mentioned, optimization parameters not only depend on the SNR, but also on the channel model. Fig. 5.6 shows the parameter a_1 obtained for five different channel models: AWGN, i.i.d. Rayleigh, i.i.d. Rice with line-of-sight $K = 10$, the mobile DVB-NGH channel with user speed 60 km/h and the Modified Guildford Model (MGM) without log-normal fading. Results show a similar tendency than the obtained for SISO (see Fig. 3.3). In AWGN, the parameter has its peak value at around 14 dB SNR, and the condensation is maintained for a wider range of low SNRs, compared to other channels. In i.i.d. Rayleigh, the curve gets smoother, keeping a similar value over the whole SNR range from 11 to 22 dB. Despite the Doppler introduced (33.3 Hz, 60 km/h), a similar behavior can be observed with the DVB-NGH mobile channel, as well as with MGM. The result with i.i.d. Rice is a middle term between AWGN and i.i.d. Rayleigh, since the channel provides better estimations due to the LoS ($K = 10$), but still introduces fading. We use the i.i.d. Rice channel in next sections.

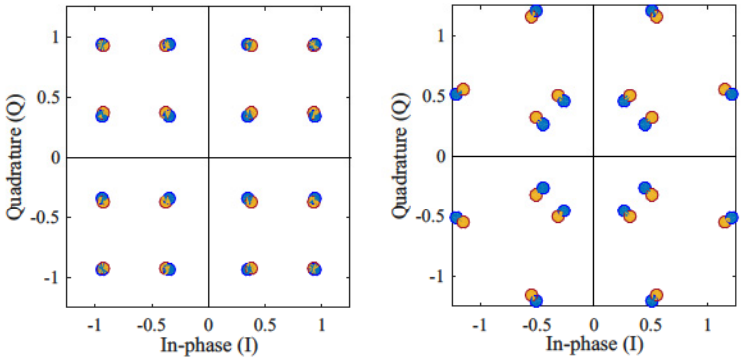


Figure 5.7: Different 16NUCs optimized for i.i.d. Rice channel and CR 4/15. Left part: 1D-NUC (blue) vs. 1D-MA-NUC (orange). Right part: 2D-NUC (blue) vs. 2D-MA-NUC (orange).

5.1.2 Re-optimization without Power Imbalance

In Chapter 3, constellations were designed seeking the maximum BICM capacity for a large range of SNRs. Afterwards, the target SNR of each particular NUC was selected for a CR according to the SNR of the waterfall region. For MIMO, we follow a different methodology. Constellations designed for SISO are not optimum for MIMO anymore, since they were designed for a different SNR and channel model. However, they still keep a good capacity gain, due to the shifting produced when doubling the number of antennas. Note that, in this dissertation, the same transmission power used in SISO is split into the two antennas. When doubling the transmission power, the result changes. In following examples, NUCs optimized for specific CRs and SISO are taken as initial parameters to optimize. A re-optimization process is then performed, where the SNR of the waterfall region is again selected considering a 2×2 MIMO scheme.

In this section, 16NUCs are shown as an example of application. When transmitting the same uniform 16QAM constellation in both antennas, and using a CR 4/15, the minimum SNR necessary to achieve a BER $\leq 10^{-4}$ in i.i.d. Rice channel is 7.6 dB. This value is taken as the SNR target for optimization. If a 1D-16NUC is used instead of QAM, which was already optimized for SISO (where the SNR target for i.i.d. Rice channel is 2.7 dB), the BICM capacity is practically maintained. The optimization parameter for SISO is $a_1 = 2.72$. Based on this parameter, it is possible to re-optimize the constellation considering all configurations selected in previous sections, e.g. same constellation in both antennas and the use of a MMSE demapper. The obtained 1D-MA-16NUC constellation slightly increases the BICM capacity, and modifies the optimum parameter $a_1 = 2.48$. However, the BICM capacity increase is not

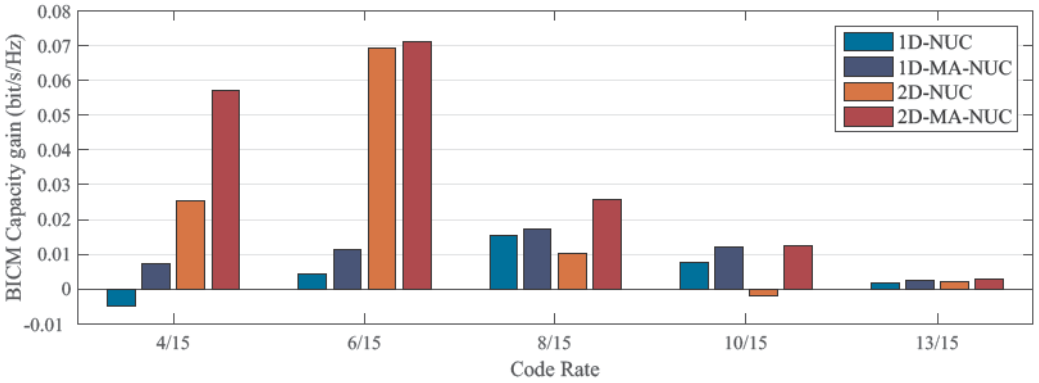


Figure 5.8: BICM capacity gain of 1D/2D-16NUC and 1D/2D-MA-16NUC over QAM, for i.i.d. Rice channel model and five representative CRs.

significant, since the DoF with these constellations is just one, simplifying the optimization process. With 2D-NUCs, there are more DoF to optimize, and therefore the capacity increase achieved is higher. A re-optimized 2D-NUC in this case achieves additional improvements, but still not significant. Fig. 5.7 depicts the different 1D- and 2D-MA-NUCs designed (orange), compared to the original NUCs from SISO (blue). As Fig. 5.7 shows, similar constellations are obtained despite the re-optimization.

Fig. 5.8 shows the BICM capacity gains with respect to QAM for the four different 16NUCs considered: 1D-NUC, 2D-NUC, 1D-MA-NUC and 2D-MA-NUC. Five representative CRs are selected from ATSC 3.0 [15]: 4/15, 6/15, 8/15 10/15 and 13/15. The CR 2/15 is not evaluated, since the same capacity gain is achieved for all constellations. At low SNRs, 16NUCs tend towards QPSK, regardless of the number of dimensions in which the optimization is done. The same does not occur with the rest of cases explored. For medium CRs, two different considerations can be made. First, the MA-NUC capacity gain over single-antenna NUCs is always higher, but almost negligible. Second, the 2D gain over 1D is also higher. This already happened in SISO, where 2D-NUCs changed towards a Gaussian shape that approaches better the channel characteristics. For high CRs, the capacity gains obtained are tiny. Coding tends to unity where no redundancy bits are employed. In this case, uniform separations between symbols ensure the minimum distances between them, minimizing the errors as much as possible, so the best possible constellation is similar to QAM. In general, one can affirm that the capacity gains achieved are not significant, and turn into slight performance gains, as shown in Section 5.2.

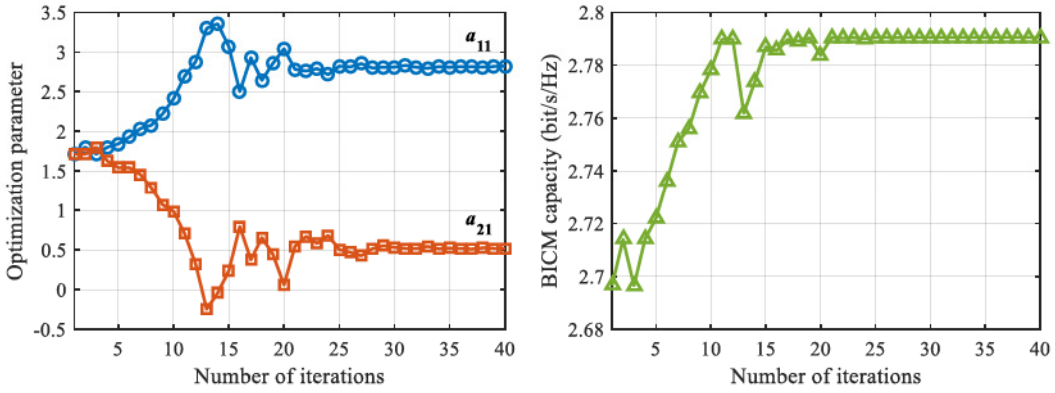


Figure 5.9: Optimization parameters for the two 16NUCs transmitted using a CR 4/15, and a PI of 6 dB. Initial parameters from SISO.

5.1.3 Re-optimization with Power Imbalance

In this section, the same re-optimization process is applied but with a PI between the two streams transmitted. An imbalance between both streams can be intentionally generated in transmission by operators to facilitate the use of dual polar MIMO operations in specific networks [76]. For this study, we modify the power allocated at each transmit antenna as detailed in Chapter 2. PI is included as part of the channel to provide a generic approach that takes into account the intentional imbalances introduced at the transmitter. From the receiver point of view, both transmitted streams experience different SNRs, thus requiring different asymmetric NUCs and using different optimization parameters a_{11} and a_{21}.

Fig. 5.9 shows the re-optimization process for the two 1D-16NUCs transmitted using a CR 4/15, and a PI of 6 dB. The SNR target considered for i.i.d. Rice channel and a CR 4/15 is 7.6 dB. Fig. 5.9 clearly depicts how both parameters follow different tendencies, almost symmetric, which also result in distinct optimized constellations. Note that the parameter obtained for the second antenna acquires a value $a_{21} = 0.5$, lower than the unity. That means that the resulting constellation symbols in a single I/Q component are exchanged. Therefore, bits are mapped to symbols in a different way than the first antenna, which employs a regular Gray-mapping. The resulting constellations in both antennas for CR 4/15, and using 1D and 2D optimization, are shown in Fig. 5.10. It can be observed that more condensed constellations are obtained for the second MIMO stream, which has lower signal power.

Fig. 5.11 depicts the BICM capacity gains with respect to QAM for a PI of 6 dB. The same representative CRs are used. As occurred without PI, the

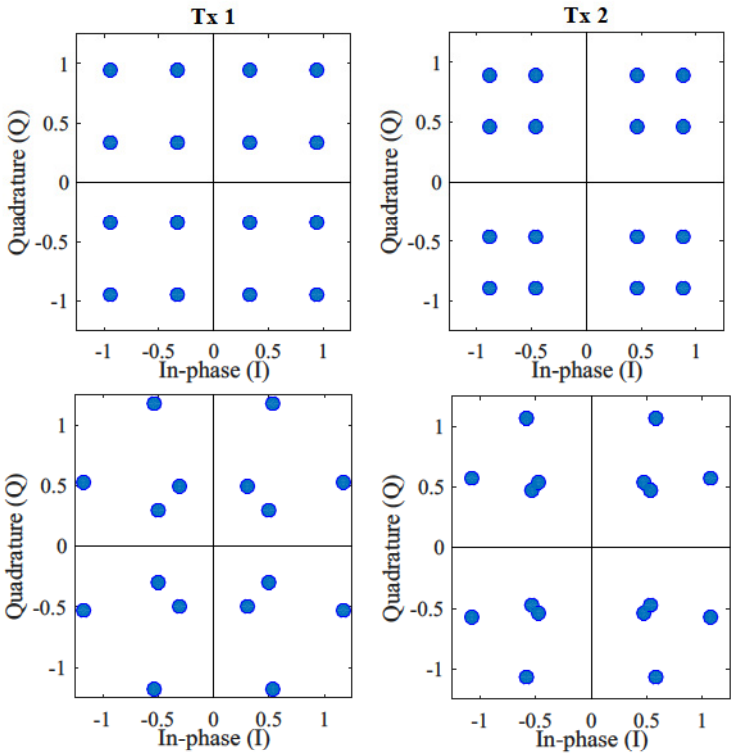


Figure 5.10: Different 16-MA-NUCs optimized for i.i.d. Rice channel and CR 4/15. 1D-NUC (top) and 2D-NUC (bottom) are shown for both transmitters.

same capacity gain and therefore the same resulting NUCs are achieved for a CR 2/15. Although different transmission powers are considered, both antennas still experience very low SNRs, tending towards the same condensed MA-NUC. The highest gain is obtained for a CR 4/15. The use of a different MA-NUC per antenna that is adapted independently to each stream, and therefore to the power imbalance introduced, increases significantly the capacity compared to regular NUCs. SISO constellations that do not consider the power imbalance condition and are optimized for a different SNR can even introduce an additional loss. This is the case when using 1D-NUCs for the CR 4/15 or 2D-NUCs for the CR 10/15. For high CRs such as 13/15, the capacity gains obtained are negligible, with similar MA-NUCs obtained for each antenna. Compared to the optimization without PI, no difference is observed for this specific CR.

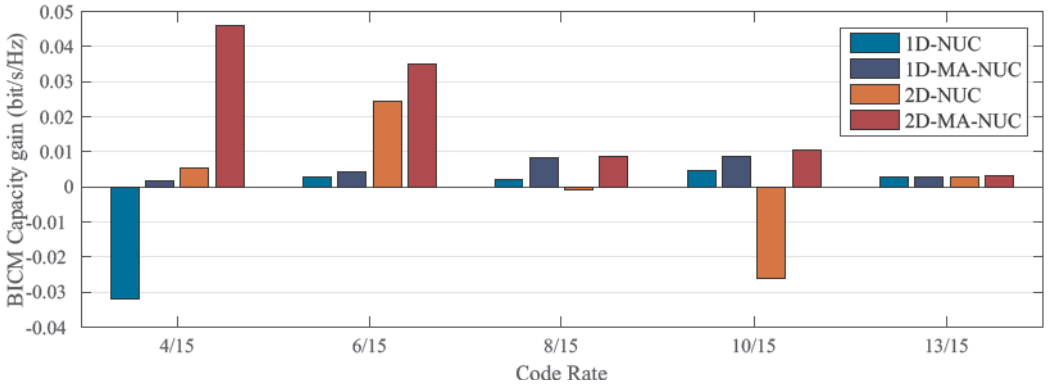


Figure 5.11: BICM capacity gain of 1D/2D-NUC and 1D/2D-MA-NUC over QAM, for i.i.d. Rice channel model and five representative CRs, PI = 6 dB.

5.2 Performance Evaluation of Multi-Antenna Non-Uniform Constellations

5.2.1 Transmission without Power Imbalance

The design and implementation of MA-NUCs only affect the mapping and demapping processes. In this section, the ATSC 3.0 specification was used for the rest of blocks implemented in both transmitter and receiver. NUCs for SISO, optimized in Chapter 3 are also used for comparison. MMSE equalization followed by two ML demappers was considered in all cases. A LDPC code length of 64800 bits was used, with bit and frequency interleavers activated [15]. Ideal channel estimation and an XPD of 6 dB are also considered. The complete transmit to receive simulation chain is defined in Appendix A.

Fig. 5.12 presents the performance achieved using the 1D- and 2D-MA-16NUCs designed for an i.i.d. Rice channel without PI. Fig. 5.12 also shows the performance of those constellations that initially were designed for the same CR and channel model, but for a SISO configuration. Two main conclusions can be extracted from this figure. First, 2D-NUCs always obtain same or better gains than 1D-NUCs. This result is very well aligned with the BICM capacity gains obtained in Section 5.1. As occurred with SISO, 2D-optimization permits the symbols a higher freedom to reach their optimum position, thus obtaining higher gains. Second, we can affirm that MA-NUCs do not provide significant gains compared to original NUCs for this case, due to the array gain considered in the optimization process when doubling the number of antennas. MIMO transmissions without PI require the same constellation in both antennas, since both streams experience similar channel conditions. Therefore, constellations

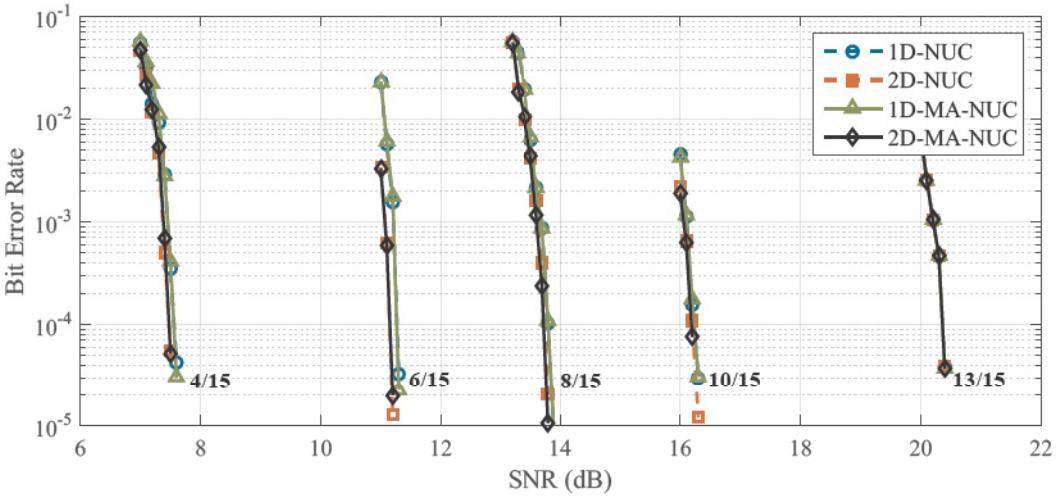


Figure 5.12: Performance (dB) of 1D/2D-16NUC and 1D/2D-MA-16NUC, for i.i.d. Rice channel model and five representative CRs, PI = 0 dB.

optimized for SISO are almost optimum for MIMO as well. Note that the performance gains over QAM are very similar to those obtained in SISO.

5.2.2 Transmission with Power Imbalance of 6 dB

MA-NUCs are effective only when exploiting a particular PI between antennas, and for specific CRs. Fig. 5.13 shows an example for a PI of 6 dB and a CR 4/15. As can be observed, NUCs optimized for SISO do not give any performance gain compared to QAM. In fact, the 1D-NUC used entails a performance loss higher than 0.1 dB. A re-optimization that considers the PI permits to adapt the constellations to the new channel, obtaining an additional gain.

Gains provided for the representative CRs can be found in Fig. 5.14. This result is well-aligned with the capacity results obtained in Section 5.1.3. The use of a different 2D-MA-NUC per antenna that is adapted independently to each stream, and therefore to the power imbalance introduced, reduces in approximately 0.1 dB the minimum SNR required, compared to regular 2D-NUCs. In general, results are aligned with the BICM capacity results. For instance, a performance loss is introduced when using 1D-NUCs for the CR 4/15 or 2D-NUCs for the CR 10/15, since SISO constellations do not consider the power imbalance condition. For high CRs such as 13/15, the capacity gains obtained are very low, and do not depend on the use of MA-NUCs or single-antenna NUCs. Compared to the performance results without PI, lower SNR gains are obtained, but the use of MA-NUCs is effective for some CRs,

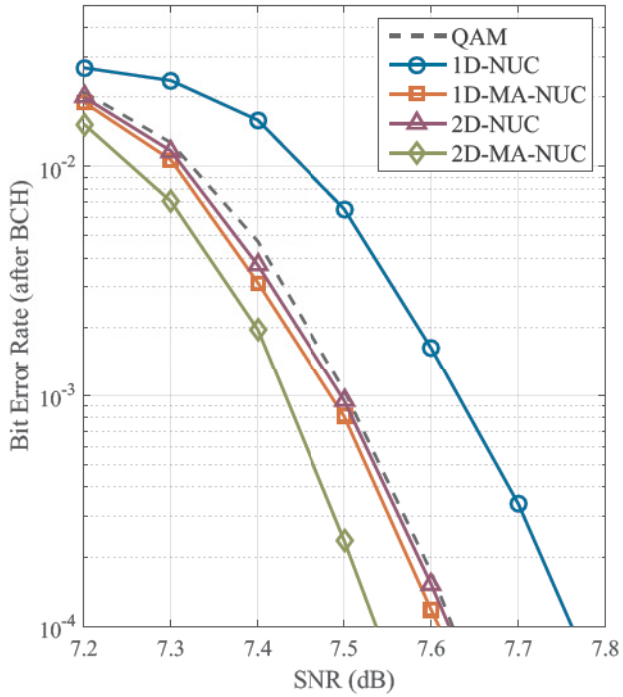


Figure 5.13: Performance comparison of QAM, 1D/2D-16NUC and 1D/2D-MA-16NUC. CR 4/15 and PI = 0 dB, for i.i.d. Rice channel model.

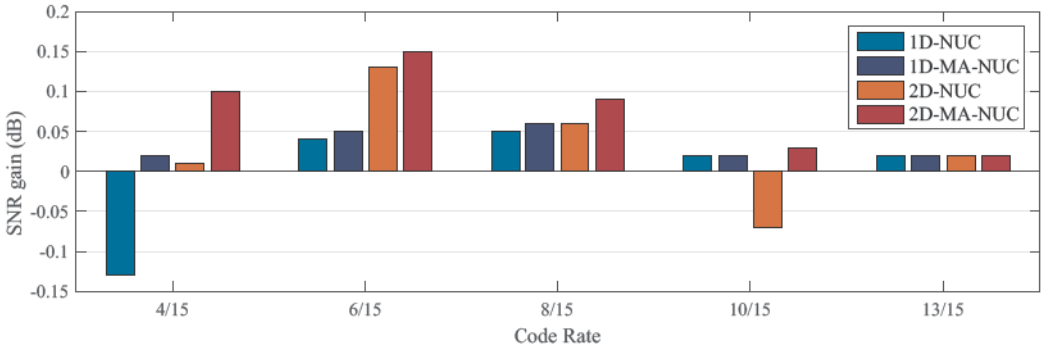


Figure 5.14: Performance gain (dB) of 1D/2D-16NUC and 1D/2D-MA-16NUC over QAM, for i.i.d. Rice channel model and five representative CRs, PI = 6 dB.

achieving additional gains and avoiding performance loss for the use of a NUC not optimized for the SNR under study. As future work of this dissertation, MA-NUC optimization should be extrapolated to higher constellation orders, where larger performance gain are expected to be achieved.

5.3 Demapping Complexity Analysis

As a generic analysis, in this section we consider 2D-NUCs with cardinality points M of 16, 64, 256, 1024 and 4096 for a MIMO system, where 8, 12, 16, 20 and 24 bits per symbol are transmitted, respectively. Although 1k-2DNUC and 4k-2DNUC constellations are not considered in the rest of the thesis, the idea is to show the complexity implications when using 2D-NUCs and MIMO. As done in the rest of this chapter, it is assumed a number of transmit and receive antennas $N_T = N_R = 2$. The complexity is defined as the number of distances or visited nodes to be computed in four different demapping schemes:

- Optimum ML
- ZF/MMSE equalization with optimum ML
- Max-log
- Sphere decoder with fixed complexity

Note that sphere decoders with variable complexity are out of the scope of this thesis. The optimum ML demapper needs to calculate all possible distances. Since it is assumed that only two transmit antennas N_T are used, the complexity can be obtained as M^2. The same applies to max-log, since all distances need to be computed. ZF and MMSE linear equalizers transform the joint MIMO demapping process into independent single-antenna demapping blocks. In a 2×2 MIMO system, the ML demapper is transformed into two independent ML demappers with complexity M, so the number of distances calculated is only $2M$. The complexity using ZF or MMSE equalizers is reduced to 75%, 87.5%, 96.8%, 99.2%, 99.8% and 99.9%, for 8NUC, 16NUC, 64NUC, 256NUC, 1024NUC and 4096NUC, respectively.

When using fixed sphere decoders such as SFSD, the complexity is drastically reduced as well. The complexity in this case is $M + (\log_2 M)^2$. In a first step, the SD algorithm calculates the distances for a single antenna, i.e. M nodes. Then, the SIC solution is applied to those nodes, reaching the $(\log_2 M)$ sub-optimal hard solutions. The second term is related to the output LLRs calculated from those solutions [98]. Compared to ML or max-log, the reduction is extremely high. The complexity reduction of SFSD compared to ML or max-log becomes especially effective for high orders of constellation. The complexity using ZF or MMSE equalizers is reduced to 73.4%, 87.5%, 97.5%, 99.5%, 99.8% and 99.9%, for 8NUC, 16NUC, 64NUC, 256NUC, 1024NUC and 4096NUC, respectively. The number of visited nodes using all considered demappers are shown in Table 5.1 and Fig. 5.15.

	ML / max-log	ZF / MMSE	SFSD
Complexity	M^2	$2M$	$M + (\log_2 M)^2$
16NUC	256	32	32
64NUC	4096	128	100
256NUC	65536	512	320
1kNUC	$1.04 \cdot 10^6$	2048	1124
4kNUC	$1.67 \cdot 10^7$	8192	4240

Table 5.1: Number of distances/nodes computed in a 2×2 MIMO system with 2D-NUCs.

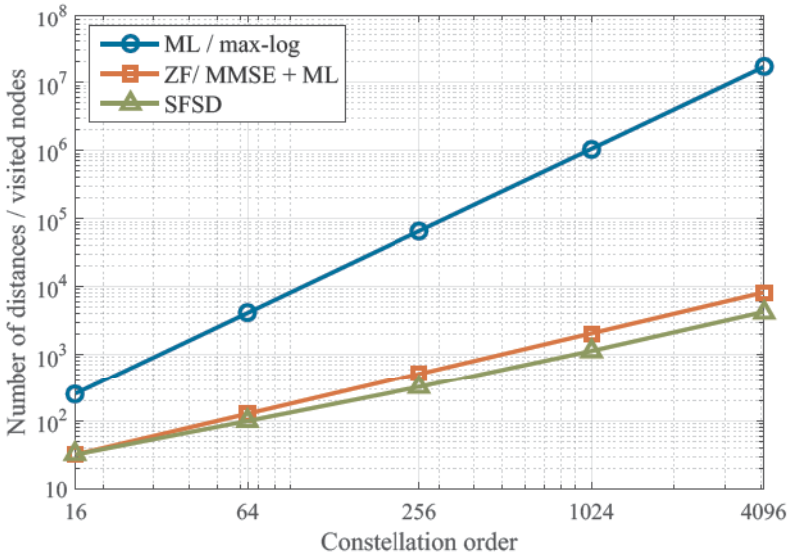


Figure 5.15: Number of distances or nodes visited with all considered demappers for 2D-NUCs.

5.4 Fixed Sphere Decoder for Two-Dimensional NUCs in MIMO

Two different alternatives are considered in this thesis, i.e. linear equalizers and sphere decoders. The best option of the two methods depends on the constellation order considered. However, linear equalizers introduce a performance loss that becomes especially high at high CRs [82]. On the other hand, SD demappers achieve a sub-optimum max-log performance and provide a similar complexity reduction than linear equalizers, as shown in Fig. 5.15. Therefore, a good option to better approach the performance vs. demapping complexity trade-off is the use of sphere decoders with fixed complexity.

In this thesis, we consider the particular case of SFSD. With SFSD, it is necessary to perform a quantization step called SIC that needs to be performed in separated I and Q components [80]. With 1D-NUCs, thanks to the squared shape, both components can be separated. However, this is not possible with 2D-NUCs. To facilitate the use of this demapper with 2D-NUCs, this section proposes an efficient pre-processing approach based on the Voronoi regions for the SIC quantization step [88]. The proposed technique is compared afterwards with the optimum ML and max-log demappers in terms of system performance. The proposed method obtains up to 97.5% of complexity reduction using 64NUCs, with a degradation lower than 0.1 dB and 0.7 dB compared to max-log and ML respectively. While results focus on 2D-NUCs for MIMO, the conclusions reached in this part of the thesis apply to all mobile communication systems, including unicast point-to-point (p-t-p) transmissions.

5.4.1 Successive Interference Cancellation

In MIMO systems, SIC is a particular subset of linear detectors [80]. SIC calculates the QR decomposition of the channel realization matrix $\mathbf{H}$ [109], where $\mathbf{Q}$ and $\mathbf{R}$ are an orthogonal and triangular matrix, respectively. It iteratively obtains an estimate of the received component from a single antenna. The estimated symbol will be used to obtain the components of the remaining antennas, as shown in Eq. 5.6.

$$\hat{s}_m = \Gamma \left\{ \frac{z_m - \sum_{i=m+1}^{N_R} R_{m,i}\hat{s}_i}{R_{m,m}} \right\}, m = N_R, ..., 1 \tag{5.6}$$

where $\hat{s}_m$ is the quantified estimated symbol from the m^{th} antenna, z_m is the received symbol multiplied by $\mathbf{Q}^H$, and $(\cdot)^H$ refers to the Hermitian operation. Γ refers to the function that gives the quantized value from a continuous input. With QAM and 1D-NUCs, estimated complex symbols are separated into real and imaginary parts, and associated to the nearest value in each dimension. The only difference using QAM or 1D-NUCs is the use of a uniform or a non-uniform quantizer. However, using 2D-NUCs, the quantization is no longer direct, since constellations do not have a squared shape and I/Q components cannot be separated. A new method is required, in order to allow SIC to work with these new constellations, and is presented in the following section.

5.4.2 Voronoi Regions Selection Algorithm

In mathematics, a Voronoi diagram is a partitioning of a plane into regions based on distances to the points in a specific subset of the plane [110]. For

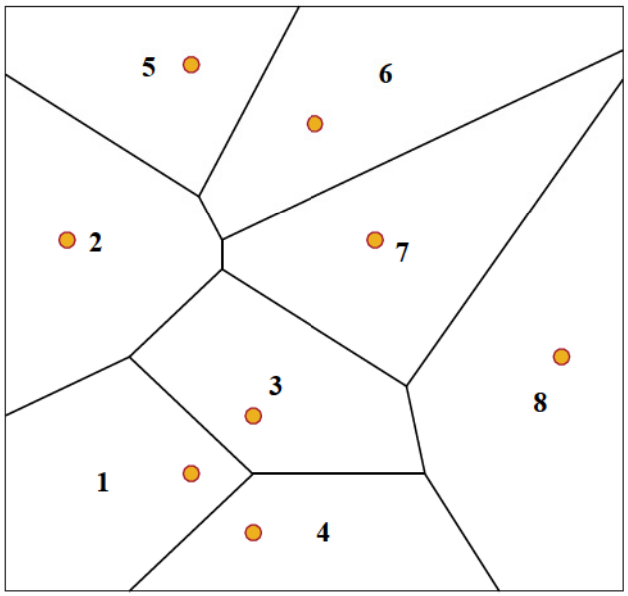


Figure 5.16: Voronoi regions calculated for 8 random points in a complex space, where each region takes an entire value associated to each point.

each constellation symbol, there is a corresponding Voronoi region in the constellation diagram consisting of the closest points to that symbol. Fig. 5.16 shows an example of the Voronoi regions calculated for 8 different positions generated randomly. Let X be a metric space with distance function d. Let I be a set of indexes and let $(P_i)_{i\in I}$ be an ordered collection of symbols in the space X. The Voronoi region R_i associated to the symbol P_i is the set of all points in X whose distance to P_i is lower than their distance to the other symbols P_j, where j is any index different from i. This can be seen in Eq. 5.7. The Voronoi diagram is simply the tuple of cells $(R_i)_{i\in I}$.

$$R_i = \{x \in X | d(x, P_i) \leq d(x, P_j), j \neq i\} \tag{5.7}$$

The proposed method is based on this mathematical approach, and is called Voronoi Regions Selection (VRS). The algorithm consists of two different phases: the first phase calculates a Look-Up Table (LUT), from the Voronoi regions associated to a given NUC. This phase is only done once, before the communication takes place, and the LUT gets stored at the receiver. In the second phase, the receiver, which is already running, loads the LUT in order to receive the signal with VRS and SFSD demapping. In practice, the LUT is equivalent to an image, where each pixel has an integer value associated. The received symbol is assigned to a particular pixel, and the corresponding value

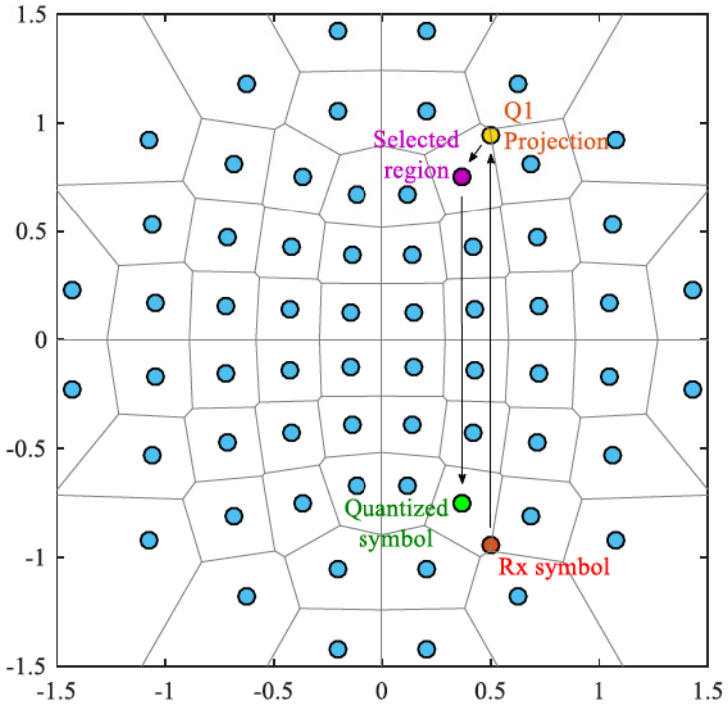


Figure 5.17: Example of Voronoi regions calculated for a 2D-64NUC, optimized for a SNR of 20 dB.

is related to a constellation symbol, as shown in Fig. 5.17. Since constellations retain up-down and left-right symmetry, only the first quadrant needs to be stored. The other three quadrants can be derived by just changing the sign of real and imaginary parts of the received symbol. A LUT with squared shape has been selected as a compromise to accommodate different distributions of NUC constellation symbols, for practical implementations in real receivers. The LUT corresponding to every possible 2D-NUC used in a certain specification, e.g. ATSC 3.0, could be calculated beforehand and uploaded to the receiver memory.

The memory usage for a LUT depends on two different variables: the number of cells or pixels in one of the two I/Q axis considered (k), which determines the total LUT size ($k \times k$), and the number of bits (b) assigned to each value/pixel of the LUT stored. The parameter b is directly associated to the constellation size and only has memory implications. The maximum number of regions to store is a quadrant of the constellation, i.e. $M/4$, being M the number of symbols. Hence, the amount of bits can be calculated as $\lceil b = \log_2(M/4) \rceil$. For instance, using a non-condensed 64NUC with $b = 4$ and $k = 40$, the stored LUT requires 6.40 Kbits. In case of condensation, the

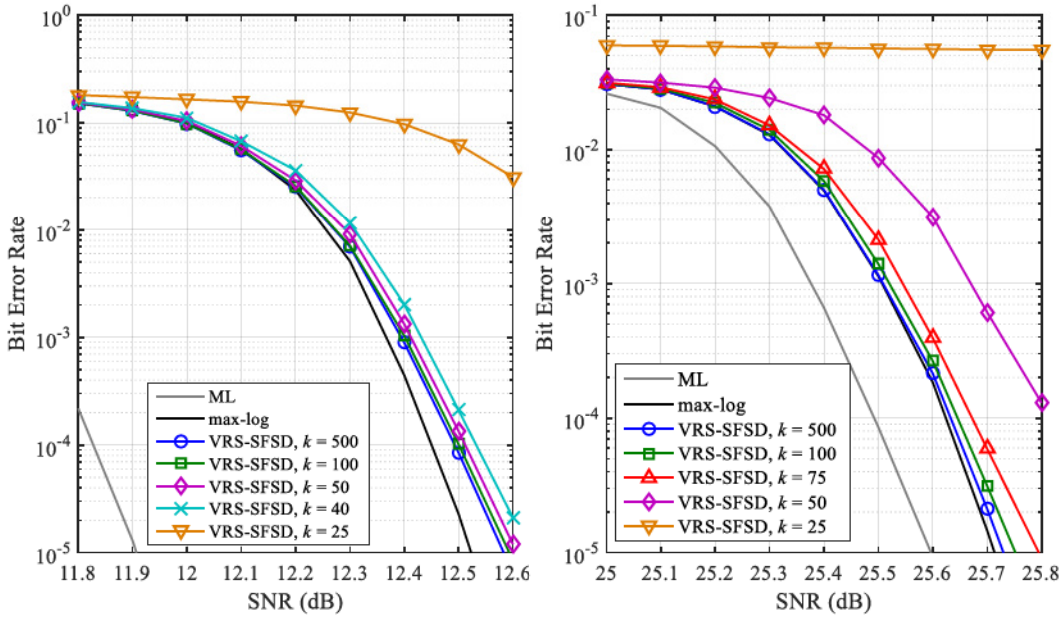


Figure 5.18: VRS with SFSD performance as a function of k, compared to ML and max-log. 64NUCs are used in each antenna. CRs 5/15 (left) and 13/15 (right).

number of regions can be further reduced, as proposed in [104]. For example, using a 64NUC optimized for a CR 2/15, the number of regions is reduced to $M = 4$, so the number of bits required is only $b = 2$.

To calculate the LUT, three steps are required. In the first step, the constellation symbols are grouped in clusters and removed, since they hinder the calculation of the Voronoi Regions. This step introduces an insignificant loss in performance, since lineal Euclidean distances among condensed symbols in normalized NUCs are almost negligible, lower than 10^{-2} [104]. In order to detect clusters, an array L with polar coordinates (radius and angle) is defined, for each constellation symbol. The algorithm evaluates each element in L individually. The difference is obtained for two threshold variables, ρ_{TH} (radius) and α_{TH} (angle in radians). This step was already explained in Chapter 4, Section 4.2.2 (CSR algorithm). In the second step, the Voronoi Regions are calculated, and each region is numbered. The LUT is created and filled by assigning a particular binary value with b bits to each Voronoi region. Finally, in a third step, a morphological filter is applied to the LUT in order to fill the possible gaps between regions.

In a following real transmission, the LUT previously calculated is loaded. For every received symbol, the SFSD demapper needs to perform the quantization step. Then, the received symbol is transformed to the first quadrant, and

	16NUC 5/15	16NUC 13/15	64NUC 5/15	64NUC 13/15
k	18	25	40	75
Number of regions	4	4	12	16
Memory (Kbits)	0.65	1.25	6.40	22.50

Table 5.2: Minimum k and required memory for VRS

the corresponding Voronoi region is retrieved from the LUT, as Fig. 5.17 depicts. Finally, the associated closest symbol is obtained and the SFSD demapping process continues, using the whole constellation.

5.4.3 Resolution vs. Performance Trade-Off

As an example of application, this section provides some illustrative performance simulation results about the use of VRS with SFSD, compared to ML and max-log demappers. A LDPC code length of 64800 bits was used. Bit, time and frequency interleavers from ATSC 3.0 were employed [34]. We use 16NUCs and 64NUCs with CRs 5/15 and 13/15 in a spatial multiplexing MIMO 2x2 system, for an i.i.d. Rayleigh channel, where co-polar antennas are considered. The entries of the channel matrix are independent amongst each other, with zero-mean. An XPD of 6 dB is assumed, with independent time realizations between symbols [86]. Ideal channel estimation was used. For the VRS method, different values for parameter k were evaluated. Note that the method VRS with SFSD and an infinite k provides max-log performance.

Fig. 5.18 shows the performance of the proposed method for 64NUC with finite k values. As Fig. 5.18 depicts, a minimum value for k of 40 and 75 is necessary to obtain a performance loss under 0.1 dB compared to max-log. Two different factors affect the dependency on the CR. With low CRs, the higher error correction capability of the LDPC code allows to cope with a lower number of cells. In addition, the condensation of the NUC reduces the amount of regions to be considered in the VRS quantization of closest symbols. Note that, compared to ML, the proposed method introduces a performance loss of 0.7 dB for CR 5/15 and 0.2 dB for CR13/15. Additional results for 16NUC are depicted in Table 5.2. The number of regions and memory requirements to store the LUT are provided as well. As Table 5.2 shows, both the number of LUT cells and memory required increase with constellation order and CR.

5.5 Conclusion

In this chapter, a NUC re-optimization process is performed for 2×2 MIMO communications. The use of several antennas modifies both the channel model and the SNR range in which the constellations work. Additional features are introduced with this technology, such as the power imbalance (PI), cross-polar discrimination (XPD), or different demappers. The optimized constellations are called multi-antenna non-uniform constellations (MA-NUC). Without PI, we have shown that optimizing the same MA-NUC in both antennas provides similar results than optimizing separated constellations in the two antennas independently. It is better just to optimize a single constellation in this case, halving the degrees of freedom for optimization. Similar optimization parameters have been obtained for MMSE and ZF equalizers as well, while drastically reducing the demapping complexity. Different MIMO channel models have been analyzed, obtaining close results. In general, the re-optimization for MIMO has shown that, without PI between transmit antennas, constellations original designed for SISO are also a good alternative for MIMO. This assumption was already considered in the ATSC 3.0 standardization process.

MA-NUCs are effective only when exploiting a particular PI between antennas. Using a MA-16NUC, the highest performance gain has been obtained for a CR 4/15. The use of a different constellation per antenna that is adapted independently to each stream, and therefore to the power imbalance introduced, reduces in approximately 0.1 dB the minimum SNR required, compared to regular 2D-NUCs. This represents a promising result, which should be extended to higher-order constellations, where larger performance gain are expected to be achieved.

At the receiver, an efficient solution for 2D-NUCs and MIMO systems based on Voronoi regions has been proposed as well. In multi-antenna systems, the optimum ML demapping complexity grows exponentially with the number of antennas and the constellation order. To reduce it, suboptimum demappers can be used, such as SFSD. However, SFSD demappers do not work with 2D-NUCs, since they perform a SIC quantization step that needs to be performed in separated I/Q components. The proposed method quantifies the closest symbol using Voronoi regions and allows SFSD demappers to work. Using VRS and SFSD and compared to ML and max-log demappers, the number of distances to be computed is reduced up to 87.5%, and 97.5% for 16NUC and 64NUC respectively. The highest performance loss introduced is 0.1 dB compared to max-log and 0.7 dB compared to ML demappers.

Chapter 6

Conclusions and Future Work

This dissertation has investigated and evaluated the use of non-uniform constellations (NUC) in digital terrestrial TV (DTT) systems that use bit-interleaved coded modulation (BICM). With uniform QAM constellations, the symbols are regularly spaced in the constellation diagram, i.e. with the same distance among symbols in both in-phase (I) and quadrature (Q) components. With NUCs, the gap between the BICM capacity of uniform QAM constellations and the theoretical Shannon limit is reduced, thanks to the shaping gain obtained from changing the positions of the different symbols in the I/Q space. Two different types of NUC have been investigated in this thesis. The first option is to keep the squared shape from QAM but relaxing the distribution between constellation symbols, with non-uniform distance between them. These constellations are called 1D-NUC and provide better signal-to-noise (SNR) performance results compared to QAM, without any complexity increase, since a 1D-demapper can be still used. The second option is to also relax the the square shape constraint, achieving a higher number of degrees of freedom (DoF) to optimize the symbol positions, thus achieving higher capacity gains. 2D-NUCs provide a better SNR performance than 1D-NUCs but with a higher demapping complexity, since a 2D-demapper is needed, i.e. I and Q components cannot be separated anymore. NUCs have been analyzed from both transmit and receive point of views, using either single-input single-output (SISO) or multiple-input multiple-output (MIMO) antenna configurations. This concluding chapter summarizes the main contributions of this thesis and suggests further topics of research beyond the results of this work.

6.1 Concluding Remarks

6.1.1 Non-Uniform Constellations Optimization

Different orders of one- and two-dimensional non-uniform constellations have been designed. Constellation symbols are optimized so the average BICM capacity is maximized, using the Nedel-Mead simplex algorithm [89]. The algorithm iteratively looks for the optimum constellation symbols, modifying their positions in the I/Q plane. In this thesis, 1D-NUCs from 16 to 4096 symbols were designed, while 2D-NUCs were optimized up to 256 symbols. This assumption was also taken into account in the ATSC 3.0 standardization process [15]. The optimization of higher constellation orders is not feasible for the algorithm considered. The complexity of the optimization process is extremely high and the method does not find the optimum solution, reaching local minimums that do not provide the best result.

Table 6.1 shows the maximum BICM capacity gain obtained with 1D-NUCs and 2D-NUCs for each constellation order and i.i.d. Rayleigh channel. It also depicts the performance gain obtained in terms of reduced SNR when using these constellations and the optimum Maximum Likelihood (ML) demapper. Results show that 2D-NUCs always provide gains compared to 1D. This additional gain comes from the more advanced optimization, which is worthwhile since the gains obtained are significative. Note that the use of two different channel models has been considered in a single optimization. Selecting different channel models affects the final constellation, with symbols located on the intermediate positions obtained in separated optimizations. Constellations for two transmission modes, i.e. fixed and mobile receptions, were also investigated. Since both modes require totally different SNR values, the combination is not optimum. It is better to focus on a particular SNR.

Another interesting concept is the use of condensed constellations. The idea is to transmit several symbols grouped in clusters, allowing to use more bits per symbol. In this case, the most significant bits provide similar robustness but the least significant bits are used to give additional information. On the other hand, the use of lower-order constellations allows to increase the CR, so in practice both constellations provide similar performance [34]. Another feature to take into account is power consumption. Although condensed, high-order constellations increase the power necessary to transmit all possible symbols. From this perspective, it is better to transmit low constellation orders that allow to use similar spectral efficiencies by using higher CRs.

2D-NUCs can be rotated to further increase the gain at high SNRs. The optimization process of Non-Uniform Rotated Constellations (NURC) has been described, first analyzing the performance in a single-RF transmission. Even

	Type	Constellation symbols				
		16	64	256	1024	4096
BICM capacity gain (bit/s/Hz)	**1D**	0.04	0.07	0.18	0.32	0.43
	2D	0.05	0.10	0.22	-	-
Performance gain (dB)	**1D**	0.05	0.32	0.65	1.05	1.20
	2D	0.16	0.45	0.82	-	-

Table 6.1: Maximum BICM capacity and performance gains per constellation order, for 1D- and 2D-NUCs, i.i.d. Rayleigh channel and optimum ML demapper.

though the demapping complexity is not increased, the SNR gain of NURCs in this case is not significant. The highest rotation gain is obtained for low-order constellations and high CRs, obtaining a maximum of 1.7 dB for i.i.d. Rayleigh channel using QPSK 13/15. This rotation gain comes from the fact that high CRs are not efficient for fading channels, where high-order constellations and low CRs provide better results. Note that rotation does not give any gain for AWGN channel. With multi-RF techniques such as Channel Bonding (CB) and Time-Frequency Slicing (TFS), the SNR gain is drastically increased, since I and Q components are transmitted in different RF channels. Without rotating NUCs, the higher the PI between RF channels, the larger the gain. The gain also depends on the CR and order of constellation. Regardless of the PI between RF channels, the highest gains are for very robust LDPC codes (low CR) with a low-order modulation. When applying an additional rotation, the highest gain is achieved with the largest possible CR, when using the QPSK modulation. In this case, the SNR gain obtained is up to 6.7 dB, with a PI of 9 dB. When extending the results to 4 RF channels, two additional scenarios have been considered: 3/4 and 1/4 RF channels with poor performance. The most important result derives from the second scenario, where the RF channel with poor performance obtains up to 8.7 dB of SNR gain using QPSK 13/15 (being 9 dB the maximum gain achievable). Additional results to these scenarios have been provided, when the RF channels present erasures. A 25%, 50% and 75% of erasures require CRs lower than 3/4, 1/2 and 1/4 respectively in order to repair the loss of information. With an additional rotation, the maximum CR is increased to 13/15, 9/15 and 6/15, respectively.

6.1.2 Complexity Implications at the Receiver

The use of NUCs on real receivers has different complexity implications. This thesis has investigated these constellations from two different points: demapping of constellation symbols and quantization of I/Q components or Log-

Likelihood Ratios (LLR) obtained. Specific algorithms have been also proposed as alternative solutions to minimize the problems detected.

For the first case considered, it is known that the number of distances to calculate with QAM and 1D-NUCs can be drastically reduced by using a 1D-demapper, as proposed in [26]. However, with 2D-NUCs and RCs, the demapper has to evaluate all distances in two dimensions. The algorithm proposed in this part is based on two different strategies. The first one is called Quadrant Search Reduction (QSR) and computes the LLRs discarding those distances whose probability of being computed is significantly low. It takes advantage of the symmetry that constellations provide, selecting a cluster of points to compute the LLRs. The second strategy is called Condensed Symbols Reduction (CSR), and exploits the condensation of NUCs, especially at low SNRs where some of the constellation symbols almost repeat the same position in the I/Q plane. It omits the computation of those distances which are similar to others already calculated, and replicates them. An example of application has been shown for 2D-256NUCs. Both strategies can be combined in order to reduce from 69% to 93% the number of required distances, depending on the CR, with almost no performance loss compared to the optimal ML demapper. The worst result is obtained for a high CR 13/15. The demapper can be extrapolated to the different orders of constellation considered in this thesis, i.e. 2D-16NUC and 2D-64NUC, but also to larger constellations such as 2D-1kNUC or 2D-4kNUC.

Regarding the influence of NUCs on digital quantizers, it has been shown that quantization values for QAM and NUC are different. Not only constellation symbols are modified with these constellations, but also LLRs obtained after the demapping process. To reduce the amount of bits to store at the TDIL, a new strategy based on BICM capacity maximization via the Nelder-Mead algorithm [89] has been proposed. It has been applied to both I/Q components and LLR values, selecting the option that provides better memory reduction percentages compared to conventional quantizers, for each modulation and CR. In general, non-uniform LLR quantization is the best choice in the sense of meeting the performance target with minimum memory requirements. The use of non-uniform quantizers adapted to the signal statistics provide slight improvements in terms of performance or alternatively in-chip memory savings.For the worst case considered, i.e. 256NUC with CR 13/15, a final reduction in TDIL memory of 30% compared to conventional quantizers has been achieved, when quantizing LLR values. Better results have been obtained for low-order constellations. With 16NUCs, the total memory reduction ranges from 45.8% to 58.3%. For 64NUCs, reduction percentages from 47.2% to 58.3% have been also obtained.

6.1.3 Multi-Antenna Optimization and Complexity Reduction

A re-optimization process has been performed for 2×2 MIMO communications. The use of several antennas modifies both the channel model and the SNR range in which the constellations work. Additional features need to be considered, such as power imbalance (PI), cross-polar discrimination (XPD), or linear equalizers. The optimized constellations are called multi-antenna non-uniform constellations (MA-NUC). Without PI, optimizing the same MA-NUC in both antennas provides similar results than optimizing separated constellations in the two antennas independently. It is better just to optimize a single constellation, halving the degrees of freedom for optimization. Similar parameters have been obtained for MMSE and ZF equalizers as well, while drastically reducing the demapping complexity. Channel models specific for MIMO have been analyzed, obtaining close results. In general, the re-optimization for MIMO has shown that, without PI between transmit antennas, constellations original designed for SISO are also a good alternative for MIMO. This can be extended to ATSC 3.0, where SISO constellations are used in MIMO.

MA-NUCs are effective only when exploiting a particular PI between antennas. As an example of application, 16-MA-NUCs have been optimized. The highest performance gain has been obtained for a CR 4/15. The use of a different constellation per antenna that is adapted independently to each stream, and therefore to the PI introduced, reduces in approximately 0.1 dB the minimum SNR required, compared to regular 2D-NUCs. For the considered case, more condensed constellations are obtained for the second MIMO stream, which has lower signal power and therefore lower SNR for optimization. This represents a promising result, which should be extended to higher-order constellations, where larger performance gains are expected to be achieved.

At the receiver, an efficient solution for 2D-NUCs and MIMO systems based on Voronoi regions has been proposed as well. In multi-antenna systems, the optimum ML demapping complexity grows exponentially with the number of antennas and the constellation order. To reduce it, suboptimum demappers can be used, such as Soft Fixed-Complexity Sphere Decoders (SFSD). However, SFSD demappers do not work with 2D-NUCs, since they perform a successive interference cancellation (SIC) quantization step that needs to be performed in separated I/Q components. The proposed method quantifies the closest symbol using Voronoi regions and allows SFSD demappers to work. Using this method and compared to ML and max-log demappers, the number of distances to be computed is reduced up to 87.5%, and 97.5% for 16NUC and 64NUC respectively. The highest performance loss introduced is 0.1 dB compared to max-log and 0.7 dB compared to ML demappers.

6.2 Constellation and CR Recommendation

The conclusions reached in this dissertation help to understand the benefits and drawbacks of non-uniform constellations, both in transmission and reception, with or without being combined with other techniques such as rotation, CB or MIMO. This section is meant to give advice and recommendation about the optimum NUC and CR configuration to use for some representative use cases in broadcasting. The most important aspect of broadcast transmission is the spectral efficiency provided to guarantee a set of services. The spectral efficiency is related to several aspects such as the SNR, CB, or rotated constellations. Additional parameters need to be considered at the receiver, which represent a performance-complexity trade-off. In this analysis, the SNR is selected to guarantee a bit error rate (BER) lower than 10^{-4}. The parameters to consider are listed below.

- **Spectral efficiency**. In this analysis, LDPC codes with additional Bose Chadhuri Hocquenghem (BCH) parity is considered. The spectral efficiency is calculated as:

$$\gamma(\text{bit/s/Hz}) = log_2(M) \cdot \frac{(L \cdot R) - B}{L} \tag{6.1}$$

  where L is the LDPC code length, M is the number of constellation symbols, R is the coding rate, B is the BCH parity rate.

- **Rotation gain**. Rotated constellations are used to improve the overall system performance at low constellation orders and high CRs. This feature is not critical upon selecting a modulation and CR combination, since the gain obtained comes from a poor SNR, due to the fading and the use of non-robust CR.

- **Channel bonding gain**:. The CB gain depends on three parameters: CR, order of constellation and PI. This analysis assumes 2 RF channels. Regardless of the PI between RF channels and without applying any rotation to the constellation, the highest gains are for very robust LDPC codes with a low-order constellation.

- **Demapping complexity**. Number of distances to compute at the receiver. Parameter directly related with the constellation order and the type of constellation. With 1D-NUCs, distances are calculated in separated components. With 2D-NUCs, no separation is possible, and therefore the QCSR demapper proposed in Chapter 4 is used to efficiently reduce the number of distances to calculate. With MIMO, the solution proposed in Chapter 5 is used.

Service	Bit rate required (Mbps)
SD	0.8 - 1.8
HD (1080p)	2 - 3.5
UHD (4k, HDR)	15 - 20

Table 6.2: Picture quality of services and bit rate required. H.265 video coding standard is assumed [111].

- **Implementation loss**. Some inter-carrier interference can be caused by the phase noise values of receiver tuners, especially for high-order constellations. This parameter also comprehends differences between ideal and real receiver algorithms [28]. This analysis assumes no implementation loss for constellations from QPSK to 64NUC.

- **Power consumption at the receiver**. Parameter directly related to the constellation order. The use of high-order constellations increases the power necessary to demodulate all possible symbols. In this sense, the best option is to use low constellation orders that allow to use similar capacities, thanks to the use of higher CRs.

- **Signal quantization at the receiver**. The number of bits required in the TDIL are also considered as an additional feature to consider in the selection process. Overall, a lower number of bits is required when using low-order constellations with very robust CRs.

The correct selection of the parameters listed above is the key for transmitting a certain set of services the most efficient way and with the lowest complexity possible at the receiver. For a minimum SNR required, the optimum case is that which provides the best capacity but also entails low complex receive techniques, such as demapping or quantization. The selected mode must guarantee other quality parameters such as low implementation loss in real hardware receivers or low power consumption in transmission.

There is a direct relation between services required and the bit rate necessary to transmit them. According to the latest H.265 video coding standard [111], the bit rate requirements associated to a particular service are shown in Table 6.2. Notice that the bit rate is calculated as $C \times B$, where C is the capacity and B is the signal bandwidth in MHz. This analysis considers 6 MHz of signal bandwidth. Also note that the requirements for High Definition TV (UHDTV) depend on the use of complementary techniques such as High Dynamic Range (HDR) [112]. The transmission of a certain number of Standard Definition TV (SDTV), High Definition TV (HDTV) or UHDTV services depends on the particular scenario.

Use case	Fixed Rx	Mobile Rx
Selected mode	64NUC 9/15	16NUC 5/15
SNR (dB)	14.5	4.3
Bit rate (Mbps)	21.5	7.9
Services provided	6 HD 1 UHD	2 HD
Demapping complexity	30	6
Implementation loss	No	
Power consumption	Low	
Rotation gain (dB)	0	
CB gain (dB)	1.45	1.55
Quantization memory (Mbits)	9.4	5.7

Table 6.3: Modulation and CR selected for the use cases considered.

Application to Use Cases

Table 6.3 reveals an example of constellation and CR combinations recommended for transmission in several scenarios. For SISO communications, 1 UHD and 2 HD services have been assumed for rooftop fixed and portable mobile reception conditions, respectively. Channel models considered are i.i.d. Rice and DVB-NGH mobile. From Table 6.2, a single UHD service requires 20 Mbps, and 2 HD services require 7 Mbps. In case of fixed reception, a 2D-64NUC with CR 7/15 has been selected, which provides a good capacity-complexity trade-off for the bit rate required, and also requires a minimum SNR lower than 15 dB, which is suitable for this type of reception. Moreover, no implementation loss is introduced, with very low power consumption. Although no rotation gain is achieved using this mode, it gives a SNR gain of 1.45 dB when CB with SNR averaging is used. On the other hand, the selected modulation for portable reception is a 2D-16NUC with CR 5/15. Both constellation order and CR have been modified in order to reduce complexity and SNR required at the expense of a lower capacity, and therefore, a smaller number of services. Note that Layered Division Multiplexing (LDM) is not considered in this analysis, which permits to use fixed and mobile services simultaneously with high spectral efficiency.

6.3 Future work

6.3.1 High-Order Two-Dimensional Non-Uniform Constellations

In this dissertation, constellations have been optimized up to 1D-4096NUC and 2D-256NUC orders. The algorithm utilized in this thesis does not reach an optimum solution for large numbers of DoF, thus making impossible to design higher-order constellations. The optimization method needs to be improved in order to design 2D-NUCs with 1024 and 4096 symbols, achieving extremely high capacity gains compared to QAM and 1D-NUCs, as shown in [24]. In turn, performance gains provided by these constellations should be thoroughly studied. The demappers proposed in this dissertation should be used with this constellations as well, in order to reduce the demapping complexity. Another option is to consider the condensation prior to optimization, for low CRs. In such case, only clusters of symbols need to be calculated, slightly reducing the capacity obtained but drastically reducing both the DoF and the number of iterations to reach the optimum solution.

6.3.2 Further Optimization for MIMO Systems

Chapter 5 has considered a re-optimization for 2×2 MIMO systems and constellations with 16 non-uniform symbols. Results have revealed that constellations optimized for SISO can be reused for MIMO if no power imbalance between transmit antennas is introduced. The power imbalance modifies the SNR target for optimization in each antenna. In this case, additional performance gains have been obtained. The study should be extended to high-orders of constellation such as 2D-64NUC or 2D-256NUC where the demapping complexity is still feasible, especially if the proposed SFSD demapper is used. The effect of the MIMO precoder in the optimized constellation has also to be investigated.

6.3.3 The Future of Broadcasting: Constellations for 5G Communications

The future of broadcasting is expected to evolve towards new scenarios where broadcast and cellular industries with different network infrastructures and business models are brought together to form a single converged network. This would enable an optimum use of the existing wireless infrastructure and spectrum [113]. Work is ongoing in the Third Generation Partnership Project (3GPP) to improve the efficiency of TV broadcast service delivery using fourth generation (4G) LTE networks. Thanks to LTE broadcast, the concepts used

in recent standards such as optimized NUCs, as well as novel concepts could be considered. NUCs can provide important gains thanks to the uplink that provides additional information on channel conditions, thus adapting to the SNR and providing an optimum capacity.

NUCs should be also introduced in the fifth generation (5G) of mobile communications for broadcasting purposes. The introduction of 5G broadcast also requires to study the most promising candidate 5G new modulation techniques, such as Frequency and Quadrature Amplitude Modulation (FQAM) or Offset Quadrature Amplitude Modulation (OQAM), in terms of increased capacity and performance. FQAM is a combination of Frequency Shift Keying (FSK) and QAM [114]. From the transmitter point of view, the use of FQAM should be further investigated and combined with NUCs. The use of this new proposal would not require a simple ML demapper in order to calculate the LLR values. In this sense, a new demapper that computes the LLRs for both the constellation and the frequency component needs to be studied. Regarding OQAM, it performs a time shift of half the inverse of the sub-channel spacing between the real and imaginary parts of a complex symbol. This constellation is combined with Filter Bank Multi-Carrier (FBMC) [115] to reduce the out-of-band interference levels and avoid the use of a guard interval (cyclic prefix) which represents an overhead for OFDM. The use of non-uniform distances between real and imaginary parts should be carefully studied in this new context. Other innovative 5G air-interface technologies to be considered that may affect the design process of these constellations are: massive MIMO [116], i.e. the use of a large number of transmit antenna elements to perform narrow two-dimensional beamforming; and Non-Orthogonal Multiple Access (NOMA), which is equivalent to LDM and allows simultaneously to use the same frequency resources for more than one transmission [117].

Appendix A

Physical Layer Simulator

The results presented in this dissertation have been obtained making use of a Physical Layer (PHY) simulator that assesses the performance and capacity gains of non-uniform constellations, among other features. This appendix presents the simulator in detail, which is based on the ATSC 3.0 specification and adapted for the particular studies carried out in this thesis. A similar architecture has been taken for the implementation of 2×2 MIMO transmissions. This simulator was implemented and used during the standardization process of the ATSC 3.0 specification [15]. The different blocks that define the complete simulator were validated with other participants in this process. The simulator is formed by five main components: parameters initialization, transmitter, channel models, receiver and error measurement, as shown in Fig. A.1. From the initial configuration introduced to the simulator, the parameters necessary to use in the simulator are pre-loaded. This includes from basic parameters such as the modulation, CR, FFT size or SNR; to more complex configurations such as interleaving indexes or LDPC matrixes. Once parameters are loaded, the core simulator starts, and no additional configuration is needed. The core simulator is formed by the transmitter, channel and receiver. At the end of the simulations, two possible options for error measurement are available: SNR performance in terms of bit and frame error rate, or mutual information calculation. The common transmit to receive diagram as well as channel models utilized for SISO and MIMO are presented in following sections.

A.1 Transmitter Block Diagram

Fig. A.2 depicts the generic transmitter used in this dissertation for simulation purposes. Blocks in black show the generic transmit SISO simulator, which is

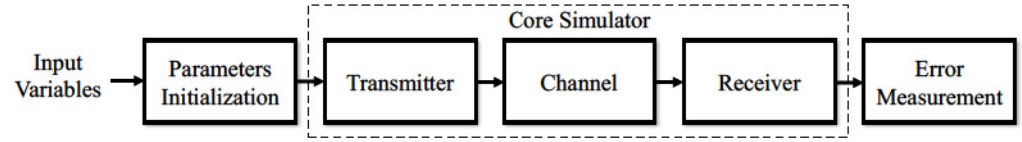


Figure A.1: Generic PHY simulator block diagram.

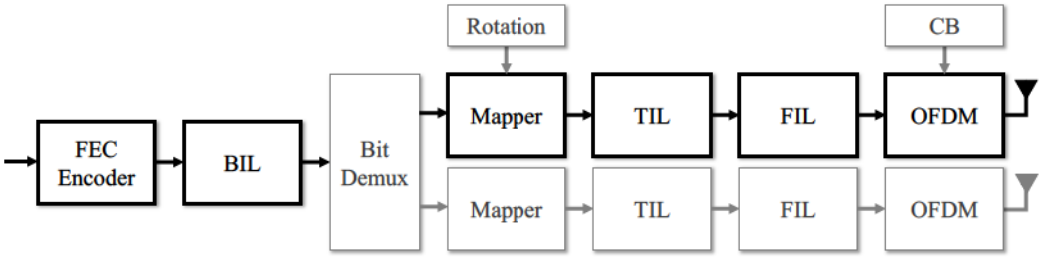


Figure A.2: Generic transmitter block diagram for SISO and MIMO used in the PHY simulator.

formed by the concatenation of FEC coding, bit interleaving, mapping, time and frequency interleaving, and waveform generation. Blocks in grey represent optional technologies additionally implemented. For MIMO, encoding and bit interleaving are jointly performed for both streams, while mappers, frequency and time interleavers, and waveform generators are applied separately. In addition, a bit demultiplexer is needed before demapping. The simulator also allows to rotate constellations, or to divide the data into two different channels with channel bonding, by simply activating or deactivating some additional parameters.

Forward Error Correction (FEC)

The PHY simulator implements forward error correction based on a concatenation of the baseband packet payload (data bits) with size K_{PAY}, an outer code (BCH) that introduces M_{OUT} additional parity bits, and a inner code (LDPC) with M_{IN} parity bits. In total, the output FEC frame has size L bits, as Fig. A.3 shows. The simulator employs LDPC inner codes from ATSC 3.0 [35]. For SISO, there are two different LDPC code lengths defined, i.e. $L = 16200$ bits (short codes) and $L = 64800$ bits (long codes). For MIMO, only the long code is specified. ATSC 3.0 permits to use a set of 12 coding rates from 2/15 to 13/15, with step 1/15. Therefore, there is a total amount of 24 different LDPC configurations to select. Note that, although ATSC 3.0 implements three options for the outer code, in this dissertation we only consider the use of BCH. The

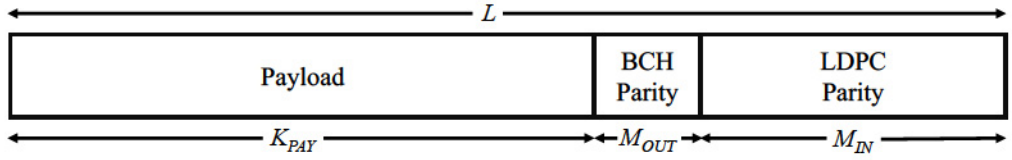


Figure A.3: Format of simulator FEC frames with BCH and LDPC coding.

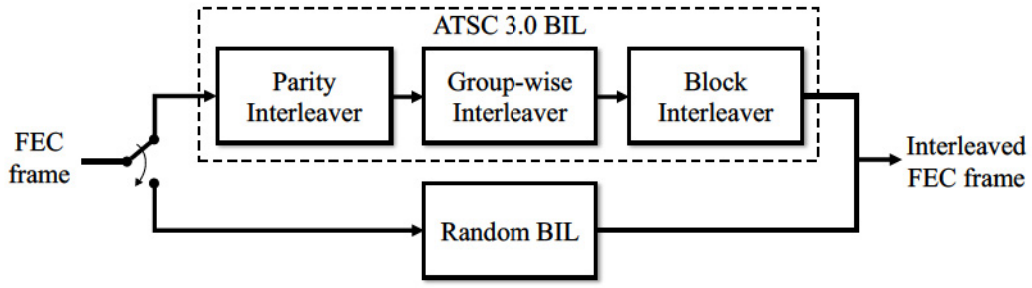


Figure A.4: Format of simulator bit interleaving. Two possible options: ATSC 3.0 or random BIL.

outer BCH code is used to lower the inherent LDPC error floor by correcting a predefined number of $M_{OUT} = 12$ bit errors .

Bit Interleaver (BIL)

Two different options are considered in the simulator for BIL, which are a random BIL and the BILs from ATSC 3.0. In both cases, the BIL block takes a FEC frame with size L as input. The output is just a bit interleaved FEC frame whose length does not change after the operation. On one hand, BILs from ATSC 3.0 consist of a parity interleaver followed by a group-wise interleaver and a block interleaver, see Fig. A.4. Bit interleaving permutations are designed so the performance with NUCs is maximized. Note that MIMO reuses the BILs from the SISO baseline and are not specifically optimized for multi-antenna transmissions. Logically, the use of these BILs with different constellations such as QAM may introduce an additional loss, since they are not designed for such case. When comparing different types of constellations, it is better to use a random BIL.

Bit Demultiplexer

In case of 2×2 MIMO transmissions, the bit demultiplexer distributes the output bits from the BIL into the two separate mappers, one per transmit antenna. With symmetric configurations, where the same order of constellation

is used in both antennas, the L bits are divided into two groups of $L/2$ bits. Odd bits are mapped to the first transmit antenna, while even bits are mapped to the second transmit antenna. With SISO, the bit demultiplexer block is not applied.

Mapper

After dividing the data into two streams (in case MIMO is selected), FEC encoded and bit interleaved bits are mapped to complex-valued constellation symbols. The input to the constellation mapping block in each stream is a FEC frame and the output is a FEC block. In addition to QPSK, the simulator implements 1D-NUCs for cardinalities from 16 to 4096 points, and 2D-NUCs for cardinalities of 16, 64 and 256 points. It also permits to use uniform QAM constellations up to 4096 symbols. The MIMO scheme allows to use either the SISO antenna baseline constellations, or those re-optimized for multi-antenna communications, called in this dissertation 1D- and 2D-MA-NUC. For the particular case of 6 and 10 bits per symbol, it also allows to use either asymmetric configurations or 8NUC and 32NUC constellations in each antenna. Constellation rotation is additionally introduced as an optional feature. The use of rotated NUCs is described in detail in Chapter 3, Section 3.3. In that section, rotation angles are also shown.

Time Interleaver (TIL)

In ATSC 3.0, time interleaving is processed in two different ways depending on the number of PLPs in which the data is transmitted. When using a single PLP mode, a convolutional TIL is used, whereas for multiple PLPs a hybrid TIL composed of cell interleaver, twisted block interleaver, and a convolutional delay-line is employed [118]. Since the use of multiple PLPs is out of the scope of this dissertation, the simulator only implements the convolutional TIL for a single PLP. The input to the convolutional TIL is a sequence of symbols coming from the mapper output. The TIL consists of N_{row} delay lines, with the k-th line having k delay elements, $k = 0, 1, ..., N_{row-1}$, and each delay element capable of storing one symbol. The number of columns N_{col} is just $N_{row} - 1$. Hence, the different inputs and outputs are controlled by two commutators, as shown in Fig. A.5, cyclically switching downwards after one cell is written in or read out, respectively.

When the interleaver is at position k, a new symbol is written to this delay line. As a first step, each delay content from this line is shifted to the immediate right position, and the content from the right-most position is output through the output commutator. In a second step, the input symbol is written to the left-most delay element of the used line. Finally, both commutators are moved

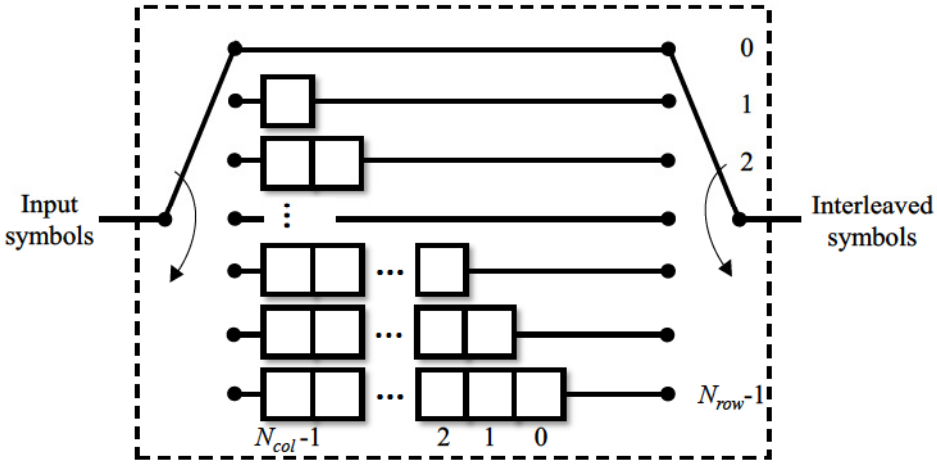


Figure A.5: Convolutional time interleaving employed in the simulator.

to the next line $k+1$. The process is cyclically repeated for N_{row}. Possible values in the simulator for N_{row} are 1024, 887, 724 and 512, which represent a time interleaving depth of 200 ms, 150 ms, 100 ms and 50 ms, respectively. Note that for MIMO scheme, both signals use the same time interleaver depth.

Frequency Interleaver (FIL)

The frequency interleaver takes data symbols coming from the TIL of one OFDM symbol, and separates error bursts occurring in the frequency domain making use of three address generators. The different address generators implemented in the simulator are also specified in ATSC 3.0, one per each FFT size available: 8K, 16K or 32K. Each address generator consists of three blocks: the toggle block, a basic interleaving sequence generator with a wire permutation, and a symbol offset generator. The main idea behind this FIL is to cyclically shift the value resulting from the combination of the output values of the three generation blocks. An additional address check block is used to validate whether the generated address is within range of the allowable addresses for the particular OFDM symbol being frequency interleaved or not. For more information, readers can refer to [119].

Waveform Generation

The waveform generator consists of a pilot insertion (in case real estimation is selected), followed by an inverse FFT and the GI insertion. Since broadcast transmissions do not use return channel, it is necessary to transmit additional

information about the channel. Several cells within the OFDM frame are modulated at a boosted power level with this information, whose value is known to the receiver. Different pilots such as scattered, continual, or edge pilots are transmitted. Information about the pilot patterns used for scattered pilots can be found in [15]. Note that no pilot insertion is needed for ideal estimation. The resulting OFDM signal is then converted into the time domain. For the resulting time-aligned frame, a guard interval is inserted to ensure that distinct transmissions with same information do not interfere with one another, such as in SFN environments. GIs from ATSC 3.0 are used in the simulator. In case channel bonding is used, the output of 2, 3 or 4 RF channels is combined to achieve greater data rates than can be achieved in one channel. The use of CB is introduced as an additional feature in this simulator, and it is explained in Chapter 3, Section 3.4.

A.2 Receiver Block Diagram

The transmitted signal is then passed through a specific channel model previously defined in the parameters initialization and taken as an input to the receiver. Fig. A.6 depicts the generic receiver used in this thesis. As done for the transmitter, blocks in black show the generic transmit SISO simulator, which is formed by the concatenation of a waveform detector (with or without using channel bonding), frequency and time de-interleaving, demapping, bit de-interleaving, and FEC decoding. Blocks in grey represent optional technologies additionally implemented. For MIMO, mappers, frequency and time de-interleavers, and waveform detection are applied separately, while decoding and bit de-interleaving are jointly performed for both streams. A MIMO demapper is needed in this case, which outputs a single bit vector from the two received complex-valued signals. The simulator also allows to perform quantization at the time de-interleaver.

From the received signal, the GI is extracted and the signal is transformed into the frequency domain. In case real estimation is used, pilots from the output signal are also extracted, and the data is stored in a new complex vector (or vectors). Frequency and time de-interleavers are then performed just using the FIL and TIL indexes stored and applied in transmission. The demapping converts the received data symbols into bits and bit de-interleaving is applied, also using the stored indexes. Finally, parity bits are extracted and the resulting bits are compared to transmitted bits in order to obtain bit and frame error rates for a particular SNR. Since most of receiver parts just need to undo the process used in transmission, only features related to this dissertation are detailed in following sections: demapping and quantization.

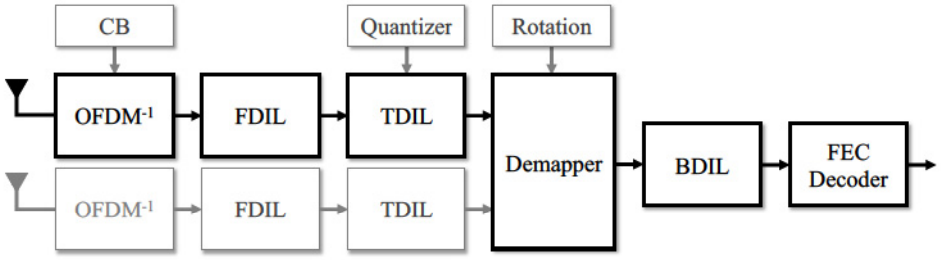


Figure A.6: Generic receiver block diagram for SISO and MIMO used in the PHY simulator.

Demapper

The simulator implements different soft-demappers that can be used in order to convert the received symbols into log-likelihood ratios. Eligible demappers depend on the number of transmit and receive antennas. The possible options considered in this simulator are the following:

- SISO:
  - Maximum-Likelihood (ML)
  - Max-log
  - Quadrant Search Reduction (QSR)
  - Condensed Symbols Reduction (CSR)
  - Quadrant Condensed Search Reduction (QCSR)
- MIMO:
  - Maximum-Likelihood (ML)
  - Max-log
  - Soft Fixed-Complexity Sphere Decoder (SFSD)
  - Soft Fixed-Complexity Sphere Decoder (SFSD) based on Voronoi regions

In addition, ML and max-log MIMO demappers can be efficiently combined with ZF and MMSE equalizers, which reduce the demapping complexity and permit the use of two independent SISO demappers.

Quantizers

Quantization is an optional operation implemented for SISO receivers. Depending on the configuration selected, quantization is performed at the TDIL before

or after the demapping takes place, i.e. demapping and TDIL blocks are accordingly reordered. Conventional receivers usually perform TDIL immediately before the demapping process takes place. In such case, constellation symbols and channel estimates are stored in order to perform time de-interleaving. In case both operations are swapped, quantization is performed in a different point of the receiver chain, i.e. output LLRs at the demapper are quantized.

A.3 Channel Models

In this section, the different channel models used throughout the dissertation are explained, for 2×2 MIMO configurations with cross-polar antennas. Note that channels described can be easily extrapolated to SISO transmissions by just simplifying the models provided, considering one antenna in both transmitter and receiver. For the considered system, the discrete received signal is modeled as in Eq. A.1.

$$\mathbf{y} = \mathbf{H}\mathbf{s} + \mathbf{w} \tag{A.1}$$

where $\mathbf{s}$ is a 2×1 transmitted vector, $\mathbf{y}$ is a 2×1 received vector, $\mathbf{H}$ is a generic channel matrix with correlated fading and cross-polar antennas, and $\mathbf{w}$ is the 2×1 additive circularly symmetric complex Gaussian noise. The matrix $\mathbf{H}$ considers that one transmit/receive antenna has vertical polarization and the other transmit/receive antenna has horizontal polarization, or vice-versa. The matrix $\mathbf{H}$ can be multiplied in turn by two additional parameters, i.e. the power imbalance between the two transmit antennas, and cross-polar discrimination (XPD) factor. The use of these parameters is explained in Chapter 2, Section 2.1.1. Note that channel models based on measurement campaigns such as the DVB-NGH mobile and MGM channels already include the XPD factor into their definitions.

AWGN Channel

The Additive White Gaussian Noise (AWGN) channel only introduces an additive circularly symmetric complex Gaussian noise where σ^2 is the noise power. The channel matrix $\mathbf{H}$ is a rectangular 2×2 matrix where all elements have value 1:

$$\mathbf{H} = \begin{bmatrix} 1 & 1 \\ 1 & 1 \end{bmatrix} \tag{A.2}$$

For SISO, the channel is simply $h = 1$. This channel, although simple, represents an accurate model for a wide set of communication channels, and can be combined with the additional channel features described above.

i.i.d. Rayleigh

When a MIMO system has sufficiently separated and equally polarized antennas with many scatters, the elements of the matrix $\mathbf{H} = \hat{\mathbf{H}}$ can be modeled using an ideal identically distributed (i.i.d.) complex Gaussian channel with zero-mean. For this channel, each matrix component can be modeled independently using the following expression:

$$\hat{h}_{ij} \sim \mathcal{CN}\left(0, \frac{1}{2}\right), i = 1, 2, j = 1, 2 \tag{A.3}$$

Fading components with those characteristics are usually known as i.i.d. Rayleigh distributed. In this dissertation, we consider that the separation between antennas is wide enough, and/or scattered components do not come from the same direction. In this case, it is said that channel components are uncorrelated [120]. Low fading correlation with cross-polarized antennas relays on the fact that the fading experimented by each polarization path possesses a low degree of correlation [27]. This channel model $\hat{\mathbf{H}}$ represents reliably scenarios where there is NLoS between the transmitter and the receiver, such as portable indoor reception scenarios.

i.i.d. Ricean

The i.i.d. Rayleigh channel can be further extended to also consider the scenario where there is LoS. This channel is called i.i.d. Ricean channel. The LoS component can be modeled using Eq. A.4.

$$\bar{\mathbf{H}} = \begin{bmatrix} \exp(j\theta_{11}) & \exp(j\theta_{12}) \\ \exp(j\theta_{21}) & \exp(j\theta_{22}) \end{bmatrix} \tag{A.4}$$

where θ_{ij} is a fixed random phase uniformly distributed between $[0, 2\pi)$. The channel matrix values $\mathbf{H}$ are modified for the i.i.d Ricean channel calculation:

$$\mathbf{H} = \sqrt{\frac{K}{1+K}}\bar{\mathbf{H}} + \sqrt{\frac{1}{1+K}}\hat{\mathbf{H}} \tag{A.5}$$

where $\bar{\mathbf{H}}$ represents the LoS component, $\hat{\mathbf{H}}$ is the NLoS component, and K models the power ratio between both components. A value $K = 10$ has been used in this dissertation since it is a suitable value to represent a channel model

under rooftop fixed reception conditions [28]. Note that, if $K = 0$ is selected, then $\mathbf{H} = \hat{\mathbf{H}}$ and the i.i.d. Rayleigh channel is applied.

DVB-NGH Mobile Channel

In the DVB-NGH standardization process, three different channels were used in order to evaluate the performance of the MIMO system proposed in a realistic scenario with mobile or portable reception. These channels were extracted from a measurement campaign carried in Helsinki in 2010. The specific channels permit to model three different scenarios, i.e. outdoor mobile, outdoor portable and indoor portable reception. In this dissertation, only mobile reception with high speed is considered. For additional information on the other two channels defined, readers can refer to [121]. The time domain channel model for the considered MIMO configuration is expressed in Eq. A.6.

$$\mathbf{H}(t,\tau) = \begin{bmatrix} h_{11}(t,\tau) & h_{12}(t,\tau) \\ h_{21}(t,\tau) & h_{22}(t,\tau) \end{bmatrix} \tag{A.6}$$

where $h_{ij}(t,\tau)$ is the impulse response between the jth transmit antenna and the ith receive antenna, t is the time domain, and τ is the delay. The channel model can be decomposed into LoS and NLoS components, and expressed in vector form as in Eq. A.7.

$$vec(\mathbf{H}^T(t,\tau)) = \bar{\mathbf{h}}\delta(t) + \sum_{n=1}^{8} \sqrt{\mathbf{R}_n}\hat{\mathbf{h}}_{w,n}\delta(t-\tau_n) \tag{A.7}$$

where $\bar{\mathbf{h}}$ is the LoS term, and the summation over the eight taps $\hat{\mathbf{h}}$ represents the NLoS term. For the nth tap, the covariance matrix $\mathbf{R}_n$ describes the correlation between the channel paths, and $\hat{\mathbf{h}}_{w,n}$ is the i.i.d complex Gaussian random vector of size 2×1.

DVB-NGH models are based on a power delay profile of 8 taps, with high cross-polarization discrimination X, and a concrete K factor. In particular, the DVB-NGH mobile channel assumes $X = 4$ and $K = \infty$ for the first tap, i.e. only LoS component is considered. The power delay profile for the DVB-NGH mobile channel is presented in Table A.1. It includes for each tap an excess delay, and co-polar/cross-polar power gains.

Note that the cross-polar gain $\sigma^2_{12}(\tau_n) = \sigma^2_{21}(\tau_n)$ can be easily calculated from the co-polar gain and the X factor as $\sigma^2_{11}(\tau_n) - 6$ (dB). The spatial correlation matrix for taps $n = 2, ..., 8$ is presented below.

Tap number, n	Excess delay, τ_n (μs)	Co-polar gain $\sigma^2_{11}(\tau_n) = \sigma^2_{22}(\tau_n)$ (dB)
1 (LoS)	0	-4
2	0.1094	-7.5
3	0.2188	-9.5
4	0.6094	-11
5	1.109	-15
6	2.109	-26
7	4.109	-30
8	8.109	-30

Table A.1: Power delay profile of the DVB-NGH mobile channel [121].

$$\mathbf{R}_n = \sigma^2_{11}(\tau_n) \begin{bmatrix} 1 & 0.06 & 0.06 & 0.05 \\ 0.06 & 0.25 & 0.03 & 0.05 \\ 0.06 & 0.03 & 0.25 & 0.06 \\ 0.05 & 0.05 & 0.06 & 1 \end{bmatrix} \tag{A.8}$$

For the first tap, the energy is pure LoS, so there is no Rayleigh part to the fading. Hence, $\mathbf{R}_1 = [0]_{4x4}$. In mobile channels, the time dependent variation of the channel realizations produce frequency shifts, and therefore the Doppler effect introduced has to be taken into account. The maximum frequency shift f_D produced at the receiver is modeled with:

$$f_D = \frac{v}{c} f_c \cos(\alpha) \tag{A.9}$$

where v is the receiver speed, c is the speed of light, f_c is the RF frequency employed, and α is the angle between directions of receiver and signal. In [121], it was observed that the experimental methodology of pushing a trolley at approximately constant speed was not sufficiently accurate to produce quantitative results. Therefore, it was decided to use power spectral density also known as Jakes-Doppler spectrum to better model the Rayleigh fading taps obtained. The Jakes-Doppler spectrum is specified to be used at a particular tap in conjunction with a fixed frequency offset proportional to f_d. The spectra of each tap is shown below:

$$\begin{cases} S(f - 3f_D/4, f_D/4) & p = 2, 3 \\ S(f + 3f_D/4, f_D/4) & p = 4, 5, 6, 7, 8 \end{cases} \tag{A.10}$$

where the tap $p = 1$ is LoS, with no Doppler shift.

Tap number, n	Excess delay τ_n (μs)	Co-polar gain $\sigma^2_{11}(\tau_n) = \sigma^2_{22}(\tau_n)$ (dB)	X_n
1 (LoS)	0	-0.943	0.0303
1 (NLoS)	0	-8.11	0.0572
2	0.2632	-22.97	0.118
3	0.5264	-32.27	0.208
4	0.7896	-35.5	0.257
5	1.448	-37	0.272
6	2.501	-38.5	0.277
7	3.554	-40.88	0.288
8	4.607	-43.94	0.313

Table A.2: Power delay profile of the MGM rooftop fixed channel [70].

Modified Guildford Model

The MGM channel has been used in this dissertation to model a rooftop reception scenario, more realistic than i.i.d. Rice. It is based on the model proposed in [70] and extracted from a measurement campaign carried in Guildford (United Kingdom) [122]. The MGM channel is also made up of 8 taps, with different delays and power gains. In this case, each tap also presents a different cross-polarization discrimination value X. As occurred with the DVB-NGH channel model, the first tap is Rice distributed with K factor, and the rest are Rayleigh distributed.

The signal model in the time domain is exactly the same as for the DVB-NGH mobile channel. It is expressed in the matrix form as in Eq. A.6, and can be decomposed in LoS and NLoS components as in Eq. A.6. The particular values of the power delay profile, as well as the X factor to apply for each tap are shown in Table A.2. The spatial correlation matrix for taps $n = 1, ..., 8$ is presented below.

$$\mathbf{R}_n = \begin{bmatrix} 1 & \sqrt{X_n}/8 & 0 & 0.15 \\ \sqrt{X_n}/8 & X_n & 0 & 0 \\ 0 & 0 & X_n & \sqrt{X_n}/8 \\ 0.15 & 0 & \sqrt{X_n}/8 & 1 \end{bmatrix} \tag{A.11}$$

The MGM is characterized by a main LoS component that models low X values with overall value 0.03. The overall K factor is 5. Note that this model additionally allows to include a 5.5 dB standard deviation log-normal distributed fading contribution into the LoS component that represents various network locations. However, the use of this log-normal contribution is not included in this dissertation.

Appendix B

Optimization Algorithm

This appendix presents the algorithm used in this thesis to obtain the optimum values (constellation symbols, rotation angles or quantization reproducers), that provide the maximum BICM capacity [89] for the system model considered. It is based on the Nelder-Mead simplex method, which is one of the most widely used methods for non-linear unconstrained optimization. Although it is widely explained in [101], this appendix provides first the main statement of the algorithm. Afterwards, an example of application is provided, in which the algorithm is adapted to one of the uses cases considered, i.e. constellation optimization.

B.1 Nelder-Mead Simplex Method

The Nelder-Mead simplex method is a direct search method that endeavors to minimize a non-linear scalar function of n real variables using function values and not using any type of derivative information [123]. This method, among many others, calculates a non-degenerate simplex at each step, i.e. a geometric figure in n dimensions that has $n+1$ vertices. For each iteration, a simplex with $n+1$ vertices is associated to $n+1$ function values. Note that each vertex is directly associated to a particular combination of input parameters (inserted as a vector). One or more vertices are computed with the function values associated, and the iteration ends with bounded level sets.

The algorithm minimizes a real-valued function $f(\mathbf{x})$ for $\mathbf{x} \in \mathcal{R}^n$, being n the number of variables to optimize, and x the input parameters. Four scalar parameters are initially defined, which are directly related to the different operations or stages in which the algorithm is divided: ρ (reflection), χ (expansion),

γ (contraction) and σ (shrinkage) [101]. The original algorithm proposed in [89] states that the mentioned parameters must satisfy:

$$\rho > 0, \quad \chi > 1, \quad \chi > \rho, \quad 0 < \gamma < 1, 0 < \sigma < 1 \tag{B.1}$$

The considered expressions in Eq. B.1 comprehend a wide range of possibilities that usually is reduced by selecting concrete values for each one of the variables. The most common choices that satisfy Eq. B.1 are the following:

$$\rho = 1, \quad \chi = 2, \gamma = 0.5, \sigma = 0.5 \tag{B.2}$$

From now on, values considered in B.2 are assumed. At the beginning of the kth iteration, where $k > 0$ and K as the total number of iterations, a new simplex Δ_k is defined, along with its $n + 1$ vertices that in turn are points in $\mathcal{R}^n$. Prior to the algorithm itself, an initial simplex Δ_0 is calculated, which has associated the $n + 1$ functions necessary to start with the first stage. An additional parameter $\delta = 0.05$ is defined. The calculation is as follows:

- $\mathbf{x}_1^{(0)} = [x_{11}, x_{12}, ..., x_{1n}]$ is taken as the input vector.
- $\mathbf{x}_2^{(0)} = [(1 + \delta)x_{21}, x_{22}, ..., x_{2n}]$.
- $\mathbf{x}_3^{(0)} = [x_{31}, (1 + \delta)x_{32}, ..., x_{3n}]$.
- $\mathbf{x}_{n+1}^{(0)} = [x_{(n+1)1}, x_{(n+1)2}, ..., (1 + \delta)x_{(n+1)n}]$.

The corresponding functions $f(\mathbf{x}^{(0)})$ are then calculated, and the algorithm begins. One iteration of the Nelder-Mead algorithm is divided in the following five stages:

1. Ordering

The iteration begins by ordering the vertices as $\mathbf{x}_1^{(k)}, ..., \mathbf{x}_{n+1}^{(k)}$ so the next expression is satisfied:

$$f_1^{(k)} \leq f_2^{(k)} \leq ... \leq f_{n+1}^{(k)} \tag{B.3}$$

where $f_i^{(k)}$ denotes $f(\mathbf{x}_1^{(k)})$. Logically, since the algorithm tries to minimize $f_i^{(k)}$, vertices are ordered such as $\mathbf{x}_1^{(k)}$ is the best vertex that provides the lowest value $f_1^{(k)}$. Following the same reasoning, $\mathbf{x}_{n+1}^{(k)}$ is taken as the worst vertex, with $f_{n+1}^{(k)}$ as the maximum non-desired value. From now on, the index k is omitted for simplicity.

2. Reflection

The reflection point $\mathbf{x}_r$ is computed as follows:

$$\mathbf{x}_r = \bar{\mathbf{x}} + \rho(\bar{\mathbf{x}} - \mathbf{x}_{n+1}) = (1+\rho)\bar{\mathbf{x}} - \rho\mathbf{x}_{n+1} = 2\bar{\mathbf{x}} - \mathbf{x}_{n+1} \tag{B.4}$$

where $\bar{\mathbf{x}} = \sum_{i=1}^{n} \mathbf{x}_i/n$ is the centroid of the best n vertices (all except the worst). Thus, the associated function $f_r = f(\mathbf{x}_r)$ is calculated, and if $f_1 < f_r < f_n$, the reflected vertex is selected and the iteration ends. In the following iteration, $\mathbf{x}_{n+1}$ will be replaced by $\mathbf{x}_r$, and the process is repeated again.

3. Expansion

If $f_r < f_1$, the expansion vertex is calculated as:

$$\begin{aligned} \mathbf{x}_e &= \bar{\mathbf{x}} + \chi(\mathbf{x}_r - \bar{\mathbf{x}}) = \bar{\mathbf{x}} + \rho\chi(\bar{\mathbf{x}} - \mathbf{x}_{n+1}) \\ &= (1+\rho\chi)\bar{\mathbf{x}} - \rho\chi\mathbf{x}_{n+1} = 3\bar{\mathbf{x}} - 2\mathbf{x}_{n+1} \end{aligned} \tag{B.5}$$

The associated function $f_e = f(\mathbf{x}_e)$ is then calculated. If $f_e < f_r$, the expanded vertex $\mathbf{x}_e$ is selected and the iteration ends. Otherwise, if $f_e \geq f_r$, the vertex selected is $\mathbf{x}_r$, and the iteration ends.

4. Contraction

If $f_r \geq f_n$, two different contractions can be performed, depending on f_{n+1}.

- **Outside contraction**: if $f_n \leq f_r \leq f_{n+1}$, then calculate:

$$\begin{aligned} \mathbf{x}_{oc} &= \bar{\mathbf{x}} + \gamma(\mathbf{x}_r - \bar{\mathbf{x}}) = \bar{\mathbf{x}} + \rho\gamma(\bar{\mathbf{x}} - \mathbf{x}_{n+1}) \\ &= (1+\rho\gamma)\bar{\mathbf{x}} - \rho\gamma\mathbf{x}_{n+1} = 1.5\bar{\mathbf{x}} - 0.5\mathbf{x}_{n+1} \end{aligned} \tag{B.6}$$

  The associated function $f_{oc} = f(\mathbf{x}_{oc})$ is calculated. If $f_{oc} < f_r$, the expanded vertex $\mathbf{x}_{oc}$ is selected and the iteration ends. Otherwise, go to stage 5.

- **Inside contraction**: if $f_r \geq f_{n+1}$, then calculate:

$$\mathbf{x}_{ic} = \bar{\mathbf{x}} - \gamma(\bar{\mathbf{x}} - \mathbf{x}_{n+1}) = (1-\rho)\bar{\mathbf{x}} + \gamma\mathbf{x}_{n+1} = 0.5\mathbf{x}_{n+1} \tag{B.7}$$

  The associated function $f_{ic} = f(\mathbf{x}_{ic})$ is calculated. If $f_{ic} < f_{n+1}$, the expanded vertex $\mathbf{x}_{ic}$ is selected and the iteration ends. Otherwise, go to stage 5.

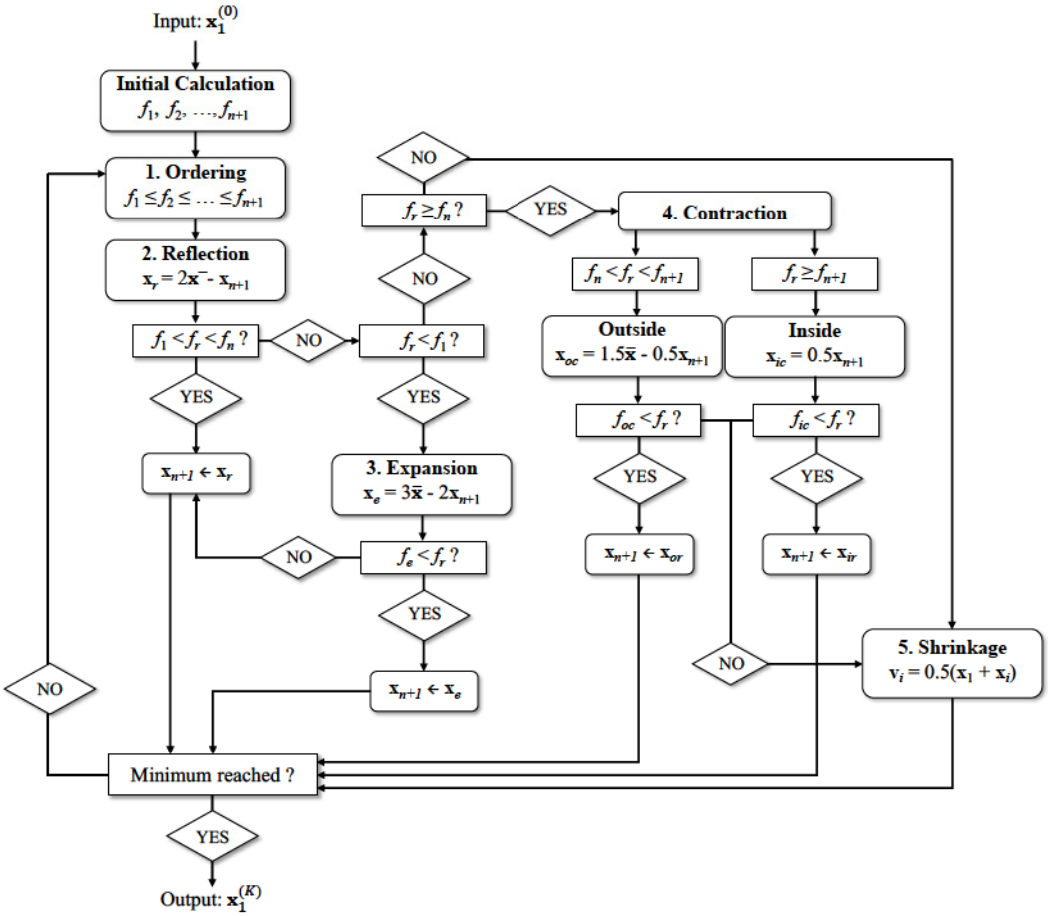


Figure B.1: Flow diagram of the Nelder-Mead optimization algorithm.

5. Shrinkage

When none of the criteria considered above is fulfilled, a shrink step is performed. The function f is evaluated at the n vertices as follows:

$$\mathbf{v}_i = \mathbf{x}_1 + \sigma(\mathbf{x}_i - \mathbf{x}_1) = (1 - \sigma)\mathbf{x}_1 + \sigma\mathbf{x}_i = 0.5(\mathbf{x}_1 + \mathbf{x}_i) \tag{B.8}$$

where $i = 2, \ldots, n + 1$. The unordered vertices of the simplex for the next iteration is $\mathbf{x}_1, \mathbf{v}_2, \ldots, \mathbf{v}_{n+1}$.

Fig. B.1 shows the complete flow diagram of the Nelder-Mead algorithm to better understand the concepts explained below. It includes the five stages considered and the possible situations that one can find during the optimization.

B.2 Application to Use Cases Considered

In this section, the Nelder-Mead simplex method is applied to one of the use cases, non-uniform constellations optimization. The input vector to the algorithm and the function to calculate for each vector considered in the different iterations are the following:

- Input vector $\mathbf{x}_1^{(0)} = \mathbf{a} = [a_1, a_2, ..., a_N]$, being $\mathbf{a}$ the symbol positions to optimize, as explained in Chapter 3.
- Function $f(\mathbf{x}_n^{(k)}) = -C_{BICM}$, following formula 2.19, defined in Chapter 2.

Since the algorithm seeks for the minimum value of the function defined, the BICM capacity is first calculated and the sign is changed afterwards. This method calculates the negative BICM capacity for each vector $\mathbf{x}_n^{(k)}$ considered, and the vector $\mathbf{x}_1^{(K)}$ in the last iteration K is finally selected, as shown in Fig. B.1.

As an example, the optimization process for a 1D-64NUC with 3 different parameters, i.e. $\mathbf{a} = [a_1, a_2, a_3]$, and a SNR = 20 dB is detailed step by step. For the case under study, an initial vector with QAM values is chosen, since the SNR selected is high and therefore, parameters will merge toward similar values. Note that indexes for the iteration k are omitted for simplicity.

$k = 0$

Using the parameter $\delta = 0.05$, an initial simplex with $n + 1 = 4$ vectors is calculated as follows:

$$\mathbf{x} = \begin{bmatrix} 3 & 5 & 7 \\ (1+\delta)3 & 5 & 7 \\ 3 & (1+\delta)5 & 7 \\ 3 & 5 & (1+\delta)7 \end{bmatrix} = \begin{bmatrix} 3 & 5 & 7 \\ 3.15 & 5 & 7 \\ 3 & 5.25 & 7 \\ 3 & 5 & 7.35 \end{bmatrix}, \qquad f(\mathbf{x}) = \begin{bmatrix} -5.814 \\ -5.800 \\ -5.776 \\ -5.822 \end{bmatrix} \tag{B.9}$$

$k = 1$

1. Ordering

$$\mathbf{x} = \begin{bmatrix} 3 & 5 & 7.35 \\ 3 & 5 & 7 \\ 3.15 & 5 & 7 \\ 3 & 5.25 & 7 \end{bmatrix}, f(\mathbf{x}) = \begin{bmatrix} -5.822 \\ -5.814 \\ -5.800 \\ -5.776 \end{bmatrix} \tag{B.10}$$

2. Reflection

$$\bar{\mathbf{x}} = \begin{bmatrix} 3.05 & 5 & 7.116 \end{bmatrix} \tag{B.11}$$

$$\mathbf{x}_r = 1.5\bar{\mathbf{x}} - 0.5\mathbf{x}_{n+1} = \begin{bmatrix} 3.1 & 4.75 & 7.233 \end{bmatrix}, f(\mathbf{x}_r) = -5.784 \tag{B.12}$$

- $f_1 < f_r < f_n$? $\rightarrow$ No.
- $f_r < f_1$? $\rightarrow$ No.
- $f_r \geq f_n$? $\rightarrow$ Yes: Contraction.
- $f_n < f_r < f_{n+1}$? $\rightarrow$ Yes: Outside Contraction.

4. Outside Contraction

$$\mathbf{x}_{oc} = 1.5\bar{\mathbf{x}} - 0.5\mathbf{x}_{n+1} = \begin{bmatrix} 3.07 & 4.87 & 7.175 \end{bmatrix}, f(\mathbf{x}_{oc}) = -5.809 \tag{B.13}$$

- $f_{oc} < f_r$? $\rightarrow$ Yes: select $\mathbf{x}_{oc}$

$$\mathbf{x} = \begin{bmatrix} 3 & 5 & 7.35 \\ 3 & 5 & 7 \\ 3.15 & 5 & 7 \\ 3.07 & 4.87 & 7.175 \end{bmatrix}, f(\mathbf{x}) = \begin{bmatrix} -5.822 \\ -5.814 \\ -5.800 \\ -5.809 \end{bmatrix} \tag{B.14}$$

$k = 2$

1. Ordering

$$\mathbf{x} = \begin{bmatrix} 3 & 5 & 7.35 \\ 3 & 5 & 7 \\ 3.07 & 4.87 & 7.175 \\ 3.15 & 5 & 7 \end{bmatrix}, f(\mathbf{x}) = \begin{bmatrix} -5.822 \\ -5.814 \\ -5.809 \\ -5.800 \end{bmatrix} \tag{B.15}$$

2. Reflection

$$\bar{\mathbf{x}} = \begin{bmatrix} 3.025 & 4.958 & 7.175 \end{bmatrix} \tag{B.16}$$

$$\mathbf{x}_r = 1.5\bar{\mathbf{x}} - 0.5\mathbf{x}_{n+1} = \begin{bmatrix} 2.9 & 4.916 & 7.35 \end{bmatrix}, f(\mathbf{x}_r) = -5.819 \tag{B.17}$$

- $f_1 < f_r < f_n$? $\rightarrow$ Yes: select $\mathbf{x}_r$.

$$\mathbf{x} = \begin{bmatrix} 3 & 5 & 7.35 \\ 3 & 5 & 7 \\ 3.07 & 4.87 & 7.175 \\ 2.9 & 4.916 & 7.35 \end{bmatrix}, f(\mathbf{x}) = \begin{bmatrix} -5.822 \\ -5.814 \\ -5.809 \\ -5.819 \end{bmatrix} \tag{B.18}$$

Although for $k = 1$ and $k = 2$ only three different stages are used, the rest are usually considered in further iterations. For instance, in this case an expansion is performed when $k = 23$ as follows:

$k = 23$

1. Ordering

$$\mathbf{x} = \begin{bmatrix} 2.944 & 4.992 & 7.279 \\ 2.945 & 4.992 & 7.277 \\ 2.943 & 4.991 & 7.281 \\ 2.945 & 4.99 & 7.28 \end{bmatrix}, f(\mathbf{x}) = \begin{bmatrix} -5.8237 \\ -5.8236 \\ -5.8234 \\ -5.8233 \end{bmatrix} \tag{B.19}$$

2. Reflection

$$\bar{\mathbf{x}} = \begin{bmatrix} 2.944 & 4.991 & 7.279 \end{bmatrix} \tag{B.20}$$

$$\mathbf{x}_r = 1.5\bar{\mathbf{x}} - 0.5\mathbf{x}_{n+1} = \begin{bmatrix} 2.943 & 4.991 & 7.276 \end{bmatrix}, f(\mathbf{x}_r) = -5.8242 \tag{B.21}$$

- $f_1 < f_r < f_n$? $\rightarrow$ No.
- $f_r < f_1$? $\rightarrow$ Yes: Expansion.

3. Expansion

$$\mathbf{x}_e = 3\bar{\mathbf{x}} - 2\mathbf{x}_{n+1} = \begin{bmatrix} 2.942 & 4.99 & 7.275 \end{bmatrix}, f(\mathbf{x}_e) = -5.8237 \tag{B.22}$$

- $f_r < f_1$? $\rightarrow$ No: select $\mathbf{x}_r$.

$$\mathbf{x} = \begin{bmatrix} 2.944 & 4.992 & 7.279 \\ 2.945 & 4.992 & 7.277 \\ 2.943 & 4.991 & 7.281 \\ 2.943 & 4.991 & 7.276 \end{bmatrix}, f(\mathbf{x}) = \begin{bmatrix} -5.8237 \\ -5.8236 \\ -5.8234 \\ -5.8242 \end{bmatrix} \tag{B.23}$$

Note that all possible $\mathbf{x}$ are very similar amongst each other for this k value, since the algorithm smoothly approaches the optimum $\mathbf{x}$ that gives the maximum BICM capacity (looking for the the minimum negative BICM capacity).

Acronyms

ATSC Advanced Television Systems Committee

ATSC 3.0 ATSC - Third Generation

AWGN Additive White Gaussian Noise

BCH Bose Chadhuri Hocquenghem

BER Bit Error Rate

BICM Bit-Interleaved Coded Modulation

BICM-ID Iteratively Decoded Bit-Interleaved Coded Modulation

BIL Bit Interleaver

CB Channel Bonding

CR Coding Rates

CIL Component Interleaver

CM Coded Modulation

CSI Channel State Information

CSR Condensed Symbols Reduction

DD Digital Dividend

DD2 Second Digital Dividend

DL Downlink

DoF Degrees of Freedom

LIST OF ABBREVIATIONS

DT Decision Threshold

DTMB Digital Terrestrial Multimedia Broadcast

DTT Digital Terrestrial Television

DVB-NGH Digital Video Broadcasting - Next Generation Handheld

DVB-T Digital Video Broadcasting - Terrestrial

DVB-T2 DVB - Terrestrial Second Generation

FBMC Filter Bank Multi-Carrier

FDM Frequency Division Multiplexing

FEC Forward Error Correction

FFT Fast Fourier Transform

FQAM Frequency and Quadrature Amplitude Modulation

FSD Fixed-Complexity Sphere Decoders

FSK Frequency Shift Keying

GI Guard Intervals

HDTV High Definition TV

HDR High Dynamic Range

i.i.d. independent and identically distributed

IMT International Mobile Telecommunications

ISDB-T Integrated Services Digital Broadcasting – Terrestrial

ISI Inter-Symbol Interference

ITU International Telecommunications Union

LDM Layered Division Multiplexing

LDPC Low Density Parity Check

LLR Log-Likelihood Ratios

LoS Line-of-Sight

LSB Least Significant Bits

LTE Long Term Evolution

LUT Look-Up Table

MA-NUC Multi-Antenna Non-Uniform Constellation

MGM Modified Guildford Model

MIMO Multiple-Input Multiple-Output

MISO Multiple-Input Single-Output

ML Maximum Likelihood

MMSE Minimum Mean Square Error

MSB Most Significant Bits

NLoS Non-Line-of-Sight

NOMA Non-Orthogonal Multiple Access

NUC Non-Uniform Constellation

NURC Non-Uniform Rotated Constellation

OAR Optimization with Additional Rotation

OBR Optimization Before Rotation

OFDM Orthogonal Frequency-Division Multiplexing

OQAM Offset Quadrature Amplitude Modulation

PHY Physical Layer

PI Power Imbalance

pdf probability density function

PLP Physical Layer Pipes

PP Pilot Pattern

p-t-p point-to-point

QAM Quadrature Amplitude Modulation

QCSR Quadrant Condensed Search Reduction

QSR Quadrant Search Reduction

RC Rotated Constellations

RF Radio Frequency

SD Sphere Decoder

SDTV Standard Definition TV

SFSD Soft Fixed-Complexity Sphere Decoders

SIC Successive Interference Cancellation

SIMO Single-Input Multiple-Output

SM Spatial Multiplexing

SNR Signal-to-Noise Ratio

SSD Signal Space Diversity

TDIL Time De-Interleaver

TDM Time Division Multiplexing

TFS Time-Frequency Slicing

TIL Time Interleaver

TV Television

UHDTV Ultra High-Definition TV

UL Uplink

UHF Ultra-High Frequency

WRC World Radiocommunication Conference

XPD Cross-Polar Discrimination

ZF Zero Forcing

3GPP Third Generation Partnership Project

References

[1] R. Beutler, *Digital Terrestrial Broadcasting Networks.* Lecture Notes in Electrical Engineering (LNEE). Springer, 2009, vol. 23.

[2] "Roadmap for the Evolution of DTT - A bright Future for TV," Digital Television Action Group (DIGITAG), Tech. Rep., 2015.

[3] W. Sami, "How can Mobile and Broadcasting Networks use Adjacent Bands?" European Broadcasting Union (EBU), Digital Dividend Technical Report, 2011.

[4] M. Fuentes *et al.*, "Coexistence of Digital Terrestrial Television and Next Generation Cellular Networks in the 700 MHz Band," *IEEE Wireless Communications*, vol. 21, no. 6, pp. 63–69, Dec. 2014.

[5] D. Gomez-Barquero, and M. W. Caldwell, "Broadcast Television Spectrum Incentive Auctions in the U.S.: Trends, Challenges, and Opportunities," *IEEE Commun. Magazine*, vol. 53, no. 7, pp. 50–56, July 2015.

[6] G. A. Reitmeier and T. R. Smith, "An Overview of the ATSC Digital Television Standard," in *International Workshop on HDTV*, Los Angeles, USA, Oct. 1996.

[7] M. Takada, and M. Saito, "Transmission System for ISDB-T," *Proceedings of the IEEE*, vol. 94, no. 1, pp. 251–256, Jan. 2006.

[8] J. Song *et al.*, "Technical Review on Chinese Digital Terrestrial Television Broadcasting Standard and Measurements on Some Working Modes," *IEEE Transactions on Broadcasting*, vol. 53, no. 1, pp. 1–7, March 2007.

[9] U. Ladebusch and C. A. Liss, "Terrestrial DVB (DVB-T): A Broadcast Technology for Stationary Portable and Mobile Use," *Procedings of the IEEE*, vol. 94, no. 1, pp. 183–193, Jan. 2006.

[10] W. Y. Zou and Y. Wu, "COFDM: an Overview," *IEEE Transactions on Broadcasting*, vol. 41, no. 1, pp. 1–8, March 1995.

[11] C. E. Shannon, "A Mathematical Theory of Communication," *Bell System Technical Journal*, vol. 27, pp. 379–423, 623–656, 1948.

[12] I. Eizmendi *et al.*, "DVB-T2: The Second Generationof Terrestrial Digital Video Broadcasting System," *IEEE Transactions on Broadcasting*, vol. 60, no. 2, pp. 258–271, June 2014.

[13] D. Gomez-Barquero, "Cost Efficient Provisioning of Mass Mobile Multimedia Services in Hybrid Cellular and Broadcasting Systems," Ph.D. dissertation, Universitat Politecnica de Valencia, Valencia, Spain, 2009.

[14] D. Gomez-Barquero, C. Douillard, P. Moss, and V. Mignone, "DVB-NGH: The Next Generation of Digital Broadcast Services to Handheld Devices," *IEEE Transactions on Broadcasting*, vol. 60, no. 2, pp. 246–257, June 2014.

[15] L. Fay *et al.*, "An Overview of the ATSC 3.0 Physical Layer Specification," *IEEE Transactions on Broadcasting*, vol. 62, no. 1, pp. 159–171, March 2016.

[16] S. I. Park *et al.*, "Low Complexity Layered Division Multiplexing for ATSC 3.0," *IEEE Transactions on Broadcasting*, vol. 62, no. 1, pp. 233–243, March 2016.

[17] N. Loghin *et al.*, "Non-Uniform Constellations for ATSC 3.0," *IEEE Transactions on Broadcasting*, vol. 62, no. 1, pp. 197–203, March 2016.

[18] A. Alvarado, E. Agrell, and A. Svensson, *On the capacity of BICM with QAM constellations.* Chalmers Publication Library, 2009.

[19] J. Massey, "Coding and Modulation in Digital Communications," in *International Zürich Seminar on Digital Communications*, Zurich, Switzerland, March 1974.

[20] G. Ungerboeck, "Channel Coding with Multilevel/Phase Signals," *IEEE Trans. Inf. Theory*, vol. 28, no. 1, pp. 55–67, Jan. 1982.

[21] H. Imai, and S. Hirakawa, "A New Multilevel Coding Method using Error Correcting Codes," *IEEE Trans. Inf. Theory*, vol. 23, no. 3, pp. 371–377, May 1977.

[22] G. Caire, G. Taricco, and E. Biglieri, "Bit-Interleaved Coded Modulation," *IEEE Trans. Inform. Theory*, vol. 44, no. 3, pp. 927–946, May 1998.

[23] A. Guillen i Fabregas, A. Martinez, and G. Caire, "Bit-Interleaved Coded Modulation," *Found. Trends Commun. Inf. Theory*, vol. 5, no. 1-2, pp. 1–153, Nov. 2008.

[24] J. Zöllner, and N. Loghin, "Optimization of High-Order Non-Uniform QAM Constellations," in *Proc. IEEE Int. Symp. Broadband Multimedia Syst. Broadcast. (BMSB)*, London, UK, June 2013.

[25] D. Gozalvez, J. J. Gimenez, D. Gomez-Barquero, and N. Cardona, "Rotated Constellations for Improved Time and Frequency Diversity in DVB-NGH," *IEEE Transactions on Broadcasting*, vol. 59, no. 2, pp. 298–305, June 2013.

[26] P. Xue, K. Bae, K. Kim, and H.Yang, "Best Candidates Based Soft-Demapper for Rotated M-QAM Constellation," in *IEEE 11th Consumer Communications and Networking Conference (CCNC)*, Las Vegas, USA, Jan. 2014.

[27] D. Vargas, "Transmit and Receive Signal Processing for MIMO Terrestrial Broadcast Systems," Ph.D. dissertation, Universitat Politecnica de Valencia, Valencia, Spain, May 2016.

[28] "Digital Video Broadcasting (DVB); Implementation guidelines for a second generation digital terrestrial television broadcasting system (DVB-T2)," ETSI TS 102 831 V1.2.1, Aug. 2012.

[29] A. Goldsmith, S. A. Jafar, N. Jindal, and S. Vishwanath, "Capacity Limits of MIMO channels," *IEEE J. Sel. Areas Commun.*, vol. 21, no. 5, pp. 684–702, June 2003.

[30] D. Tse and P. Viswanath, *Fundamentals of Wireless Communications*. Cambridge University Press, 2015.

[31] E. Zehavi, "8-PSK Trellis Codes for a Rayleigh Channel," *IEEE Trans. Communications*, vol. 40, no. 3, pp. 873–884, May 1992.

[32] A. Alvarado, "On Bit-interleaved Coded Modulation with QAM Constellations," Ph.D. dissertation, Chalmers University of Technology, Göteborg, Sweden, 2008.

[33] D. Gomez-Barquero, *Next Generation Mobile Broadcasting.* Ed. Boca Raton, FL, USA: CRC Press, 2013.

[34] L. Michael, and D. Gomez-Barquero, "Bit-interleaved Coding and Modulation (BICM) for ATSC 3.0," *IEEE Trans. Broadcast.*, vol. 62, no. 1, pp. 181–188, March 2016.

[35] K. J. Kim *et al.*, "Low-Density Parity-Check Codes for ATSC 3.0," *IEEE Trans. Broadcast.*, vol. 62, no. 1, pp. 189–196, March 2016.

[36] G. J. Foschini, R. Gitlin, and S. Weinstein, "Optimization of Two-Dimensional Signal-Constellations in the Presence of Gaussian Noise," *IEEE Trans. Commun.*, vol. 22, no. 1, pp. 28–38, Jan. 1974.

[37] J. Stott, "BICM Limits for Condensed QAM, Further Results," DVB document TM-MIMO0023, Feb. 2013.

[38] J. Stott, "CM and BICM Limits for Rectangular Constellations," White Paper 257, BBC Research and Development, Aug. 2013.

[39] B. Mouhouche, D. Ansorregui, and A. Mourad, "High Order Non-Uniform Constellations for Broadcasting UHDTV," in *Proc. IEEE Wireless Commun. Netw. Conf. (WCNC)*, Istambul, Turkey, April 2014.

[40] J. Morgade *et al.*, "Improving the DVB-T2 BICM Performance by newly Optimized Two-Dimensional Non-Uniform Constellations," in *IEEE Fourth International Conference on Consumer Electronics (ICCE)*, Berlin, Germany, Sept. 2014.

[41] T. Arafa, W. Sauer-Greff, and R. Urbansky, "Non-Uniform Signal Constellation for Iteratively Decoded Bit Interleaved Coded Modulation (BICM-ID) with Convolution and LDPC Codes," in *International Conference on Innovations in Information Technology (IIT)*, Abu Dhabi, UAE, April 2011.

[42] C. Barjau *et al.*, "Improvement of L1 Signaling Performance for DVB-T2 Using Optimized Two-Dimensional Non-Uniform Constellations," in *IEEE International Conference on Ubiquitous Wireless Broadband (ICUWB)*, Montreal, Canada, Oct. 2015.

[43] J. Stott, "Beyond NUQAM & ConQAM - Overcoming their Limitations, Especially at Lower SNRs," DVB document TM-T0007, Jan. 2014.

[44] S. Kwon *et al.*, "Simplified Non-Uniform Constellation Demapping Scheme for the Next Broadcasting System," in *IEEE Int. Symp. Broadband Multimedia Syst. Broadcast. (BMSB)*, Ghent, Belgium, June 2015.

[45] J. Barrueco *et al.*, "Low Complexity and High Order Two-Dimensional Non-Uniform Constellations for High Capacity Broadcasting Systems," in *IEEE International Symposium on Broadband Multimedia Systems and Broadcasting (BMSB)*, Nara, Japan, July 2016.

[46] B. Mouhouche, C. Barjau, and H. Lee, "Design of Non Uniform Constellations for Layered Division Multiplexing," in *IEEE International Symposium on Signal Processing and Information Technology (ISSPIT)*, Abu Dhabi, UAE, Sept. 2015.

[47] J. Montalban, "Solutions for New Terrestrial Broadcasting Systems Offering Simultaneously Stationary and Mobile Services," Ph.D. dissertation, University of the Basque Country, Bilbao, Spain, Dec. 2014.

[48] D. Gomez-Barquero, and O. Simeone, "LDM vs. FDM/TDM for Unequal Error Protection in Terrestrial Broadcasting Systems: An Information-Theoretic View," *IEEE Trans. Broadcast.*, vol. 61, no. 4, pp. 571–579, Aug. 2015.

[49] J. Boutros and E. Viterbo, "Signal Space Diversity: A Power- and Bandwidth-Efficient Diversity Technique for the Rayleigh Fading Channel," *IEEE Trans. Inform. Theory*, vol. 44, no. 4, pp. 1453–1467, July 1998.

[50] Q. Xie *et al.*, "Coded Modulation with Signal Space Diversity," *IEEE Trans. on Wireless Communications*, vol. 10, no. 2, pp. 660–669, Dec. 2010.

[51] C. A. Nour, and C. Douillard, "Improving BICM Performance of QAM Constellations for Broadcasting Applications," in *5th International Symposium on Turbo Codes and Related Topics*, Lausanne, Switzerland, Sept. 2008.

[52] D. Gozalvez, "Combined Time, Frequency and Space Diversity in Multimedia Mobile Broadcasting Systems," Ph.D. dissertation, Universitat Politecnica de Valencia, Valencia, Spain, June 2012.

[53] D. Perez-Calderon *et al.*, "Rotated Constellation Demapper for DVB-T2," *IEEE Electron. Lett.*, vol. 47, no. 1, pp. 31–32, Jan. 2011.

[54] D. Perez-Calderon *et al.*, "Simplified Rotated Constellation Demapper for Second Generation Terrestrial Digital Video Broadcasting," *IEEE Trans. Broadcast.*, vol. 59, no. 1, pp. 160–167, March 2013.

[55] S. Tomasin, and M. Butussi, "Low Complexity Demapping of Rotated and Cyclic Q Delayed Constellations for DVB-T2," *IEEE Wireless Communications Letters*, vol. 1, no. 2, pp. 81–84, April 2012.

[56] B. Hassibi, and H. Vikalo, "On the Sphere-Decoding Algorithm I. Expected Complexity," *IEEE Tans. Signal Processing*, vol. 53, no. 8, pp. 2806–2818, Aug. 2005.

[57] J. Yang *et al.*, "Max-Log Demapper Architecture Design for DVB-T2 Rotated QAM Constellations," in *IEEE Workshop on Signal Processing Systems (SiPS)*, Dallas, USA, Oct. 2015.

[58] D. Gozalvez, D. Gomez-Barquero, D. Vargas, and N. Cardona, "Combined Time, Frequency and Space Diversity in DVB-NGH," *IEEE Trans. Broadcast.*, vol. 59, no. 4, pp. 674–684, Dec. 2013.

[59] M. Makni, J. Robert, and E. Stare, "Performance Analysis of Time Frequency Slicing," in *14th ITG Conference on Electronic Media Technology (CEMT)*, Dortmund, Germany, March 2011.

[60] J. J. Gimenez, E. Stare, S. Bergsmark, and D. Gomez-Barquero, "Time Frequency Slicing for Future Digital Terrestrial Broadcasting Networks," *IEEE Trans. Broadcast.*, vol. 60, no. 2, pp. 227–238, June 2014.

[61] J. J. Gimenez, "Improved Spectrum Usage with Multi-RF Channel Aggregation Technologies for the Next-Generation Terrestrial Broadcasting," Ph.D. dissertation, Universitat Politecnica de Valencia, Valencia, Spain, June 2015.

[62] L. Stadelmeier, D. Schneider, J. Zöllner, and J. J. Gimenez, "Channel bonding for ATSC 3.0," *IEEE Trans. Broadcast.*, vol. 62, no. 1, pp. 289–297, March 2016.

[63] E. Garro, J. J. Gimenez, S. Ik Park, and D. Gomez-Barquero, "Layered Division Multiplexing With Multi-Radio-Frequency Channel Technologies," *IEEE Trans. Broadcast.*, vol. 62, no. 2, pp. 365–374, June 2016.

[64] E. Stare, J. J. Gimenez, and P. Klenner, "WIB ï¿½ A New System Concept for Digital Terrestrial Television (DTT)," in *International Broadcasting Convention (IBC)*, Amsterdam, Netherlands, Sept. 2016.

[65] J. Max, "Quantizing for Minimum Distortion," *IEEE Trans. Information Theory*, vol. 6, no. 1, pp. 7–12, March 1960.

[66] A. Gersho and R. M. Gray, *Vector Quantization and Signal Compression.* Kluwer Academic Publishers, 1992.

[67] R. M. Gray and D. L. Neuhoff, "Quantization," *IEEE Trans. Information Theory*, vol. 44, no. 6, pp. 2325–2383, Oct. 1998.

[68] A. Winkelbauer, and G. Matz, "On Quantization of Log-Likelihood Ratios for Maximum Mutual Information," in *IEEE International Workshop on Signal Processing Advances in Wireless Communications (SPAWC)*, Stockholm, Sweeden, June 2015.

[69] S. Rosati, S. Tomasin, M. Butussi, and B. Rimoldi, "LLR Compression for BICM Systems Using Large Constellations," *IEEE Trans. Communications*, vol. 61, no. 7, pp. 2864–2875, July 2013.

[70] P. Moss, "2-by-2 MIMO Fixed Reception Channel Model for Dual-Polar Terrestrial Transmission," White Paper 161, BBC Research and Development, Jan. 2008.

[71] D. Vargas *et al.*, "A MIMO-Channel-Precoding Scheme for Next Generation Terrestrial Broadcast TV Systems," *IEEE Trans. Broadcast.*, vol. 61, no. 3, pp. 445–456, Sept. 2015.

[72] J. Jang, D. H. Kim, and Y. H. Lee, "Open-Loop Precoder for Spatial Multiplexing in MIMO Channels with Phase Correlation," *IET Electronic Letters*, vol. 50, no. 23, pp. 1766–1768, Nov. 2014.

[73] S. Saito *et al.*, "8K Terrestrial Transmission Field Tests using Dualpolarized MIMO and Higher-Order Modulation OFDM," *IEEE Trans. Broadcast.*, vol. 62, no. 1, pp. 306–315, Jan. 2016.

[74] P. Fertl, J. Jaldï¿½n, and G. Matz, "Performance Assessment of MIMO-BICM Demodulators Based on Mutual Information," *IEEE Trans. Signal Processing*, vol. 60, no. 3, pp. 1366–1382, March 2012.

[75] D. Vargas, D. Gozalvez, D. Gomez-Barquero, and N. Cardona, "MIMO for DVB-NGH, the Next Generation Mobile TV Broadcasting," *IEEE Commun. Magazine*, vol. 51, no. 7, pp. 130–137, July 2013.

[76] D. Gomez-Barquero *et al.*, "MIMO for ATSC 3.0," *IEEE Trans. Broadcast.*, vol. 62, no. 1, pp. 298–305, March 2016.

[77] T. Shitomi *et al.*, "Field Experiments of Dual-Polarized MIMO-OFDM Transmission Using Non-Uniform Constellations," in *IEEE International Conference on Consumer Electronics (ICCE)*, Berlin, Germany, Jan. 2016.

[78] D. Perez-Calderon *et al.*, "Simplified Detection for DVB-NGH MIMO Decoders," *IEEE Trans. Broadcast.*, vol. 61, no. 1, pp. 84–90, March 2015.

[79] T. Shitomi *et al.*, "Evaluation of Simplified Demapping Algorithm for NUQAMs Using Urban MIMO Channel Response," in *IEEE International Symposium on Broadband and Multimedia Systems and Broadcasting (BMSB)*, Nara, Japan, June 2016.

[80] T. Kailath, H. Vikalo, and B. Hassibi, *MIMO Receive Algorithms.* Cambridge University Press, 2005.

[81] E. Viterbo and J. Boutros, "A Universal Lattice Decoder for Fading Channels," *IEEE Trans. on Information Theory*, vol. 45, no. 5, p. 1639ï¿½1642, July 1999.

[82] S. Roger, "Design and Implementation of Efficient Algorithms for Wireless MIMO Communication Systems," Ph.D. dissertation, Universitat Politecnica de Valencia, Valencia, Spain, July 2012.

[83] L. G. Barbero, T. Ratnarajah, and C. Cowan, "A Low-Complexity Soft-MIMO Detector based on the Fixed-Complexity Sphere Decoder," in *IEEE International Conference on Acoustics, Speech and Signal Processing*, Las Vegas, USA, March 2008.

[84] C. Studer, M. Wenk, A. Burg, and H. Bölcskei, "Soft-Output Sphere Decoding: Performance and Implementation Aspects," in *Asilomar Conference on Signals, Systems and Computers (ACSSC)*, Pacific Grove, USA, Nov. 2006.

[85] H. Nyquist, "Certain Topics in Telegraph Transmission Theory," *Reedited manuscript, Proceedings of the IEEE*, vol. 90, no. 2, pp. 280–305, Feb. 2002.

[86] E. Telatar, "Capacity of Multi-Antenna Gaussian Channels," *European Trans. Telecomm.*, vol. 10, no. 6, pp. 585–596, Nov. 1999.

[87] G. Strang, *Introduction to Linear Algebra.* 4th Ed. Wellesley-Cambridge Press, 2009.

[88] C. Barjau, M. Fuentes, T. Shitomi and D. Gomez-Barquero, "MIMO Sphere Decoder with Successive Interference Cancellation for Two-Dimensional Non-Uniform Constellations," *IEEE Communications Letters*, Jan. 2017.

[89] J. A. Nelder, and R. Mead, "A Simplex Method for Function Minimization," *Computer Journal*, vol. 7, no. 4, pp. 308–313, 1965.

[90] J. Barry, E. Lee, and D. Messerschmitt, *Digital Communications*. United States: Ed. Springer, 2003.

[91] D. Seethaler, G. Matz, and F. Hlawatsch, "An effcient MMSE-based Demodulator for MIMO Bit-Interleaved Coded Modulation," in *IEEE Globecom*, Dallas, USA, Nov. 2004.

[92] C. Douillard *et al.*, "Iterative Correction of Intersymbol Interference: Turbo-Equalisation," *European Trans. Telecomm.*, vol. 6, no. 5, pp. 507–511, Sept. 1995.

[93] R. Koetter, A. Singer, and M. Tuchler, "Turbo Equalization," *IEEE Signal Proc. Magazine*, vol. 21, no. 1, pp. 67–80, Jan. 2004.

[94] M. Witzke, S. Bäro, F. Schreckenbach, and J. Hagenauer, "Iterative Detection of MIMO Signals with Linear Detectors," in *Asilomar Conference on Signals, Systems and Computers*, Pacific Groove, USA, Nov. 2002.

[95] E. Agrell, T. Eriksson, A. Vardy, and K. Zeger, "Closest Point Search in Lattices," *IEEE Trans. on Information Theory*, vol. 48, no. 8, pp. 2201–2214, Aug. 2002.

[96] Z. Guo, and P. Nilsson, "Algorithm and Implementation of the K-Best Sphere Decoding for MIMO Detection," *IEEE Journal on Selected Areas in Communications*, vol. 24, no. 3, pp. 491–503, March 2006.

[97] M. O. Damen, H. E. Gamal, and G. Caire, "On Maximum-Likelihood Detection and the Search for the Closest Lattice Point," *IEEE Trans. Inf. Theory*, vol. 49, no. 10, pp. 2389–2402, Oct. 2003.

[98] L. G. Barbero, and J. S. Thompson, "Fixing the Complexity of the Sphere Decoder for MIMO Detection," *IEEE Trans. Wireless Communications*, vol. 7, no. 6, pp. 2131–2142, June 2008.

[99] J. Jalden, L. G. Barbero, B. Ottersten, and J. S. Thompson, "The Error Probability of the Fixed-Complexity Sphere Decoder," *IEEE Trans. on Signal Processing*, vol. 57, no. 7, pp. 2711–2720, July 2009.

[100] G. D. Forney Jr., and L.-F. Wei, "Multidimensional Constellations ï¿½ Part I: Introduction, Figures of Merit and Generalized Cross Constellations," *IEEE Journal on Selected Areas in Communications*, vol. 1, no. 6, pp. 877–892, Aug. 1989.

[101] J. C. Lagarias, J. A. Reeds, M. H. Wright, and P. E. Wright, "Convergence Properties of the Nelder-Mead Simplex Method in Low Dimensions," *SIAM Journal of Optimization*, vol. 9, no. 1, pp. 112–147, 1998.

[102] L. Yang, and Z. Huiyan, "Shape Preserving Piecewise Cubic Interpolation," *Applied Mathematics*, vol. 11, no. 4, pp. 419–424, Dec. 1996.

[103] M. Fuentes, J. J. Gimenez and D. Gomez-Barquero, "Optimization and Performance of Non-Uniform Rotated Constellations with Multi-RF Transmission Techniques," *IEEE Trans. Broadcast.*, vol. 62, no. 4, pp. 855–863, Dec. 2016.

[104] M. Fuentes, D. Vargas and D. Gomez-Barquero, "Low-Complexity Demapping Algorithm for Two-Dimensional Non-Uniform Constellations," *IEEE Trans. Broadcast.*, vol. 62, no. 2, pp. 375–383, June 2016.

[105] J. J. Gimenez, D. Gozalvez, D. Gomez-Barquero, and N. Cardona, "Statistical Model of Signal Strength Imbalance Between RF Channels in DTT Network," *Electronic Letters*, vol. 48, no. 12, pp. 731–732, June 2012.

[106] T. M. Cover, *Elements of Information Theory.* John Wiley & Sons Inc., 2001, pp. 336–373.

[107] A. Winkelbauer, "Blind Performance Estimation and Quantizer Design with Applications to Relay Networks," Ph.D. dissertation, Technische Universtität Wien, Vienna, Austria, Dec. 2014.

[108] J. Liang, L. Thiele, and V. Jungnickel, "On the Modelling of Polarized MIMO Channel," in *13th European Wireless Conference*, Paris, France, April 2007.

[109] G. H. Golub, and C. F. Van Loan, *Matrix Computations.* The Johns Hopkins Univesity Press, 3rd Edition, 1996.

[110] F. Aurenhammer, "Voronoi Diagrams - A Survey of a Fundamental Geometric Data Structure," *ACM Computing Surveys*, vol. 23, no. 3, pp. 345–405, Sept. 1991.

[111] G. J. Sullivan, J. Ohm, Woo-Jin Han, and T. Wiegand, "Overview of the High Efficiency Video Coding (HEVC) Standard," *IEEE Transactions on Circuits and Systems for Video Technology*, vol. 22, no. 12, pp. 1649–1668, Dec. 2012.

[112] W. Li *et al.*, "Using LDM to achieve seamless local service coverage in SFN environment," in *IEEE International Symposium on Broadband Multimedia Systems and Broadcasting (BMSB)*, Nara, Japan, July 2016.

[113] J. Calabuig, J. F. Monserrat, and D. Gomez-Barquero, "5th Generation Mobile Networks: A new Opportunity for the Convergence of Mobile Broadband and Broadcast Services," *IEEE Communications Magazine*, vol. 53, no. 2, pp. 198–205, Feb. 2015.

[114] S. Hong *et al.*, "FQAM : A Modulation Scheme for Beyond 4G Cellular Wireless Communication Systems," in *IEEE Globecom Workshops (GC Wkshps)*, Atlanta, USA, June 2013.

[115] V. Vakilian *et al.*, "Universal-Filtered Multi-Carrier Technique for Wireless Systems Beyond LTE," in *IEEE Globecom Workshops*, Atlanta, USA, Dec. 2013.

[116] E. Larsson, O. Edfors, F. Tufvesson, and T. Marzetta, "Massive MIMO for Next Generation Wireless Systems," *IEEE Communications Magazine*, vol. 52, no. 2, pp. 186–195, Feb. 2014.

[117] A. Benjebbour *et al.*, "Concept and Practical Considerations of Non-Orthogonal Multiple Access (NOMA) for Future Radio Access," in *Proc. IEEE ISPACS*, Okinawa, Japan, Nov. 2013.

[118] P. Klenner *et al.*, "Physical Layer Time Interleaving for the ATSC 3.0 System," *IEEE Trans. Broadcast.*, vol. 62, no. 1, pp. 253–262, March 2016.

[119] M. Earnshaw *et al.*, "Physical Layer Framing for ATSC 3.0," *IEEE Trans. Broadcast.*, vol. 62, no. 1, pp. 263–27, March 2016.

[120] S. M. Alamouti, "A Simple Transmit Diversity Technique for Wireless Communications," *IEEE J. Sel. Areas Comm.*, vol. 16, no. 10, pp. 1451–1458, Oct. 1998.

[121] P. Moss, T. Y. Poon, and J. Boyer, "A Simple Model of the UHF Crosspolar Terrestrial Channel for DVB-NGH," White Paper 205, BBC Research and Development, Sept. 2011.

[122] J. Boyer *et al.*, "MIMO for Broadcast-Results from a High-Power UK Trial," White Paper 157, BBC Research and Development, Jan. 2007.

[123] M. Wright, *Direct Search Methods: Once Scorned, Now Respectable.* Addison-Wesley, Numerical analysis: Proceedings of the 1995 Dundee Biennial Conference in Numerical Analysis, 1996, pp. 191–208.